Geological Magazine

www.cambridge.org/geo

Original Article

Cite this article: Wei S, Tang J, Song Y, Li B, and Dong Y (2023) Petrogenesis of Early Cretaceous volcanic rocks from the Rena-Co area in the southern Qiangtang Terrane, central Tibet: evidence from zircon U-Pb geochronology, petrochemistry and Sr-Nd-Pb–Hf isotope characteristics. *Geological Magazine* **160**: 1144–1159. https://doi.org/10.1017/S0016756823000274

Received: 21 August 2022
Revised: 14 March 2023
Accepted: 31 March 2023
First published online: 2 May 2023

Keywords:
Adakite-like dacites; Petrogenesis; Rena-Co area; Bangong–Nujiang suture zone; Tibet

Corresponding author: Shaogang Wei, Email: shaogang_wei@yahoo.com

Petrogenesis of Early Cretaceous volcanic rocks from the Rena-Co area in the southern Qiangtang Terrane, central Tibet: evidence from zircon U-Pb geochronology, petrochemistry and Sr-Nd-Pb–Hf isotope characteristics

Shaogang Wei[1,2], Juxing Tang[3], Yang Song[3], Baolong Li[3] and Yujie Dong[4]

[1]School of Materials Engineering, Changshu Institute of Technology, Changshu, Jiangsu, China; [2]National Institute of Natural Hazards, Ministry of Emergency Management of the People's Republic of China, Beijing, China; [3]MLR Key Laboratory of Metallogeny and Mineral Assessment, Institute of Mineral Resources, Chinese Academy of Geological Sciences, Beijing, China and [4]No. 5 Geological Party, Tibet Bureau of Geology and Mineral Exploration and Development, Golmud, Qinghai, China

Abstract

The subduction of the Bangong–Nujiang Ocean is important in the geological evolution of the Tibetan Plateau. In this paper, we report new zircon U-Pb age and Lu-Hf isotopic data and whole-rock elemental and Sr-Nd-Pb isotopic data for Early Cretaceous dacites from the Rena-Co area (RCA) in the southern Qiangtang Terrane (QT), central Tibet and use these data to better understand the tectonic evolution of the Bangong–Nujiang suture. LA–ICP-MS dating of zircons yields ages of 109.5 ± 0.6 Ma to 109.6 ± 0.8 Ma for the dacites from the RCA. Geochemically, these dacites are medium-K calc-alkaline and show high SiO_2 contents of 64.79–70.37 wt.%, high Sr contents of 517–598 ppm and low Y contents of 8.45–10.7 ppm, similar to those of typical adakites. Additionally, all the rocks are strongly enriched in light rare earth elements and some large ion lithophile elements (e.g. Rb, U, K and Cs) but significantly depleted in high-field-strength elements (e.g. Nb, Ta and Ti), consistent with the geochemical characteristics of arc-type magmas formed in the subduction zone. Moreover, these adakite-like dacites show whole-rock initial $(^{87}Sr/^{86}Sr)_i$ ratios of 0.705119 to 0.705491, $(^{206}Pb/^{204}Pb)_i$ ratios of 18.489 to 18.508, $(^{207}Pb/^{204}Pb)_i$ ratios of 15.591 to 15.612, $(^{208}Pb/^{204}Pb)_i$ ratios of 38.599 to 38.686, $\epsilon_{Nd}(t)$ values of −0.28 to +1.25 and single-stage Nd model ages of 642 to 818 Ma, as well as significantly positive zircon $\epsilon_{Hf}(t)$ values of 3.9–13.1, with young Hf-depleted mantle ages of 331 to 923 Ma. These geochemical and isotopic data indicate that they are most likely derived from the juvenile thickened mafic lower continental crust, which contains partial melts of metasomatized peridotite and subduction-related fluids in the magma source region. Based on previous studies and our new data, we propose that the RCA adakite-like dacites are most likely a result of the northwards subduction of the Bangong–Nujiang Ocean lithosphere beneath the southern QT during the Early Cretaceous and that a slab rollback model could explain the formation of the RCA adakite-like dacites.

1. Introduction

The Tibetan Plateau shares a long and complex geological history involving multiple episodes of spreading, subduction and continental collision in the Tethys Ocean basin. The Bangong–Nujiang suture zone (BNSZ), located between the Lhasa terrane to the south and the Qiangtang terrane (QT) to the north, extends more than 2000 km across the central Tibetan Plateau (Fig. 1a). This zone is generally considered the locus of the ancient Bangong–Nujiang Ocean (BNO) (Yin & Harrison, 2000; Kapp *et al.* 2003, 2005; Pan *et al.* 2004; Guynn *et al.* 2006; Zhang *et al.* 2012; Li *et al.* 2016; Zhu *et al.* 2016). The closure of the BNO, followed by the subsequent collision between the Lhasa and Qiangtang terranes, significantly contributed to the initial growth of the Tibetan Plateau before the Indo-Asian collision (Kapp *et al.* 2007; Shi *et al.* 2008, 2020; Zhang *et al.* 2012, 2014; Zhu *et al.* 2016; Zeng *et al.* 2021). However, intense controversies remain on the closure of the BNO, and two main versions of the final closure of the BNO have been proposed. The first hypothesis is that the BNO closed between the Late Jurassic and Early Cretaceous (ca. 160-145 Ma), mainly on the basis of the presence of an angular unconformity between the Lower Jurassic oceanic rocks (flysch deposits and ophiolites) and the Upper Jurassic–Lower Cretaceous shallow marine strata (e.g. Xu *et al.* 1985; Dewey *et al.* 1988; Yin *et al.* 1988; Kapp *et al.* 2003, 2005, 2007; Raterman *et al.* 2014). The alternative version suggests that the collision between the Lhasa terrane and QT may have occurred after the Early Cretaceous (Ca. 120-100 Ma), according to abundant Early Cretaceous

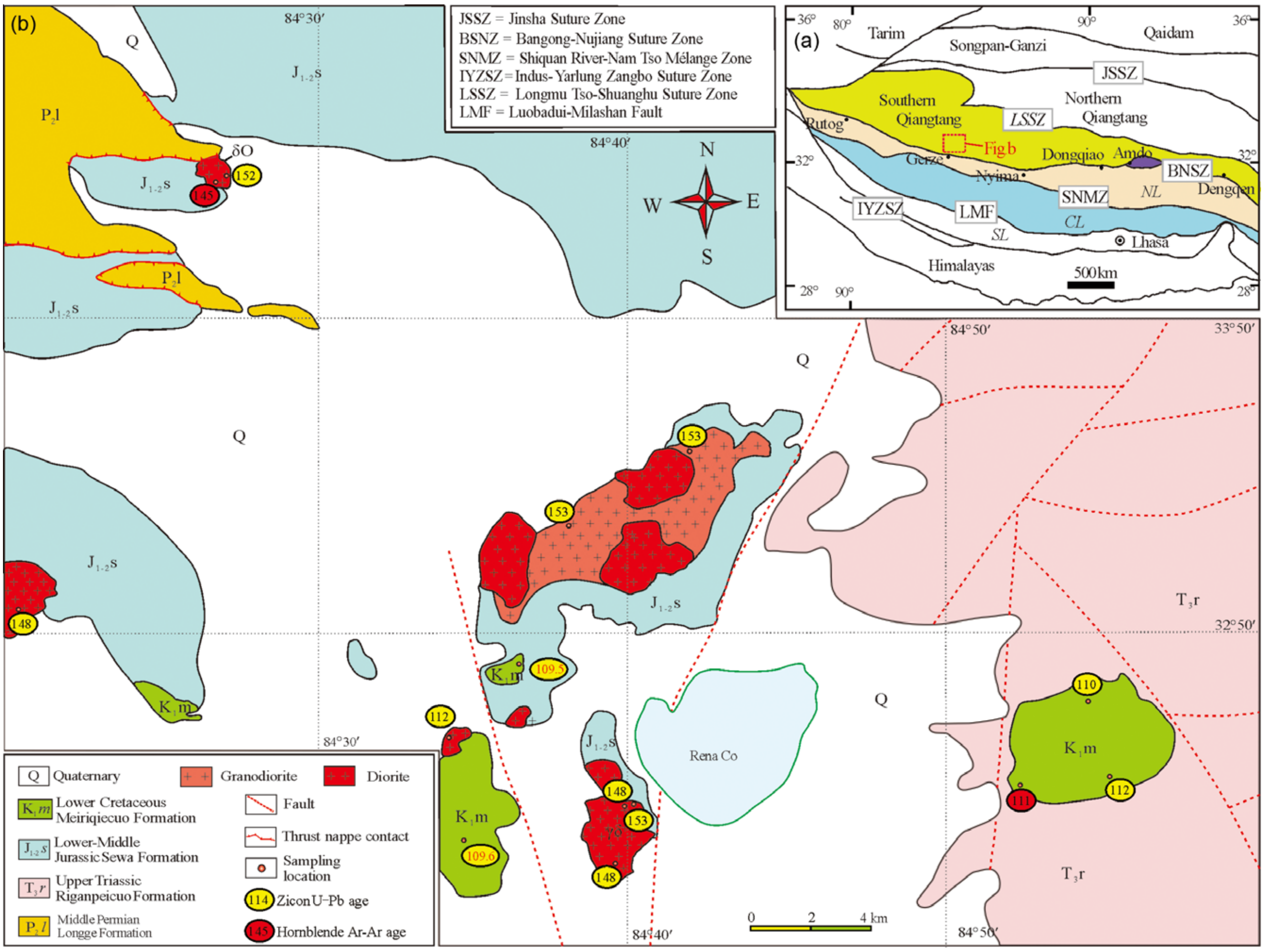

Figure 1. (Colour online) (a) Tectonic framework of the Tibetan Plateau (modified from Zhu *et al.* 2009, 2016; Sui *et al.* 2013); (b) simplified geologic map showing outcrops of magmatic rocks in the RCA, western Qiangtang, central Tibet [modified from Kapp *et al.* (2005) and Song *et al.* (2021)]. Age data in this paper are in red font; other literature age data are from Chang *et al.* (2011), Kapp *et al.* (2005), Hao *et al.* (2016*a*) and Song *et al.* (2021).

oceanic island basalt (OIB)-type rocks that are overlain by or interbedded with radiolarian-bearing chert and/or limestone, the existence of a mid-Cretaceous magmatic arc in the southern QT and palaeomagnetic data (e.g. Zhu *et al.* 2006; Bao *et al.* 2007; Baxter *et al.* 2009; Zhang *et al.* 2012, 2014; Xu *et al.* 2015; Chen *et al.* 2018; Fan *et al.* 2018; Luo *et al.* 2020; Shi *et al.* 2020).

The Rena-Co area (RCA) is located in the southern margin of the QT to the north of the BNSZ (Fig. 1b). Late Mesozoic volcanic rocks are widely distributed within this area (e.g. Kapp *et al.* 2005; Chang *et al.* 2011; Li *et al.* 2016; Wei *et al.* 2017), and this area has been a research focus in recent years (Kapp *et al.* 2005; Chang *et al.* 2011; Li *et al.* 2014*a*; Hao *et al.* 2016*a*, *b*; Song *et al.* 2021). It is well accepted that understanding Cretaceous volcanism in the southern margin of the QT is of great significance for understanding the evolution of the BNO and Qiangtang–Lhasa collisional orogeny (Yin & Harrison, 2000; Kapp *et al.* 2003, 2005; Zhu *et al.* 2016). Late Mesozoic volcanic rocks, especially the dacites of the Meiriqiecuo Formation (MF) from the RCA, could play an important role in constraining the tectonic setting at that time. However, the detailed petrogenesis of the Early Cretaceous dacites in the RCA remains unknown.

In this paper, we focus on the MF dacites from the RCA in the southern QT, central Tibet. Here, we present new zircon U-Pb ages, whole-rock major and trace element compositions, and whole-rock Sr-Nd-Pb and in situ zircon Hf isotope data for the RCA dacites. Based on our new data, we provide a new tectono-magmatic model to explain the Early Cretaceous magmatism in the southern QT and constrain the petrogenetic processes of the RCA dacites and the time of the closure of the BNO.

2. Geological background and petrographic observations

The Tibetan Plateau is composed of four continental terranes from south to north: the Himalaya, Lhasa, Qiangtang, and Songpan–Ganzi. These terranes are separated by the Indus–Yarlung Zangbo suture zone (IYZSZ), Bangong–Nujiang suture zone (BNSZ), and Jinshajiang suture zone (JSSZ) (Yin & Harrison, 2000; Shi *et al.* 2008; Zhu *et al.* 2016). The BNSZ is 20–95 km wide in a N-S direction and >2200 km long in an E-W direction and represents a geologically significant suture zone that stretches from Bangongco to the west via Gerze, Nyima, Dongqiao, Amdo and Dêngqên to the east and then turns south into the Mogok area of Myanmar (Yin & Harrison, 2000; Kapp *et al.* 2003, 2005). As the boundary of the LT and the QT, the BNSZ contains abundant Jurassic-Cretaceous flysch, mélange and scattered ophiolitic fragments (Sengör, 1979; Girardeau *et al.* 1984; Yin *et al.* 1988; Kapp *et al.* 2003). To the north of the BNSZ, the southern QT is composed of Carboniferous–Permian shelf strata along with

https://doi.org/10.1017/S0016756823000274 Published online by Cambridge University Press

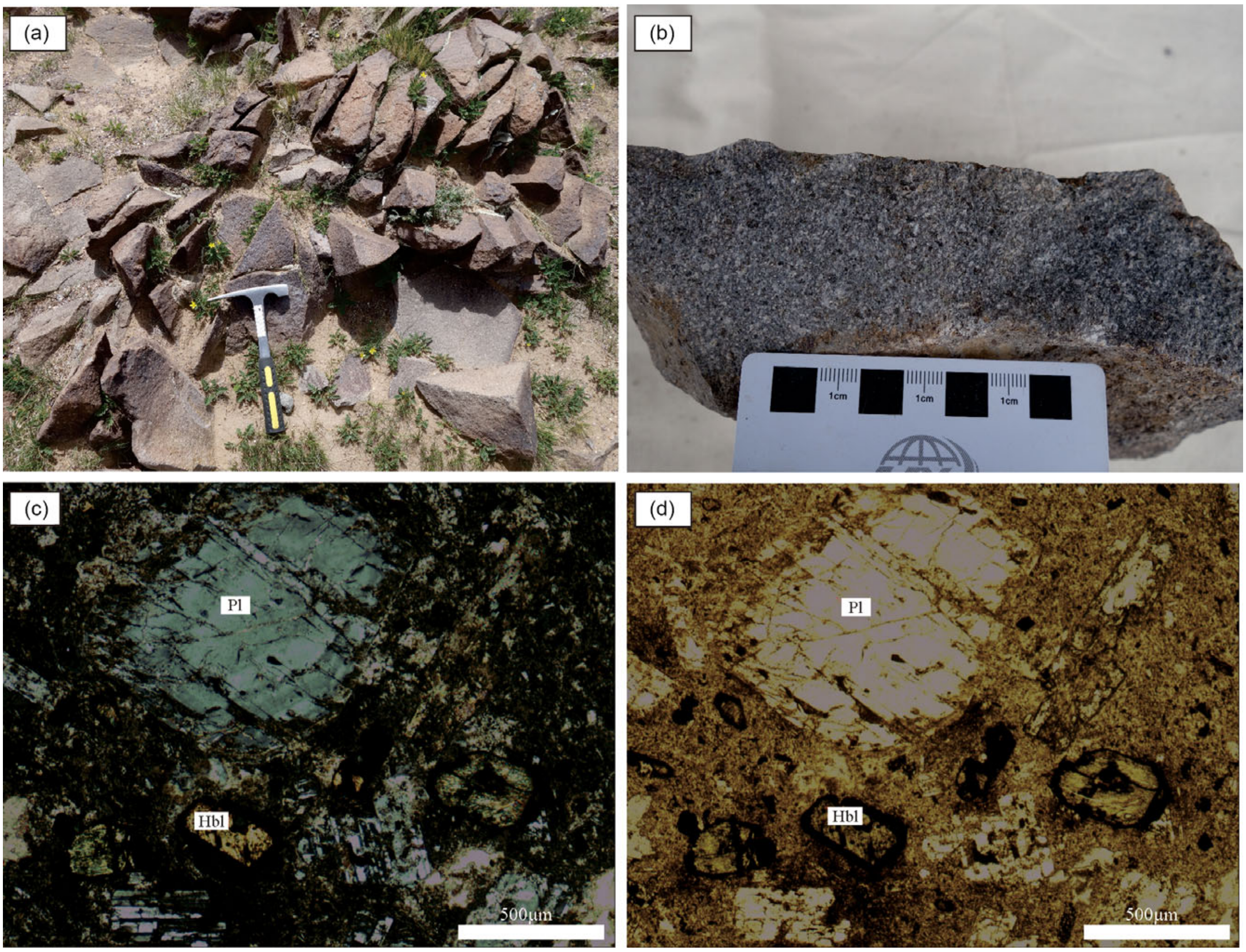

Figure 2. (Colour online) Photomicrographs showing the porphyric texture of the MF volcanic rocks collected from the RNA in the western QT, central Tibet. Note that the groundmass minerals mainly consist of plagioclase microlites, cryptocrystalline minerals and minor magnetite.

Jurassic marine rocks exposed along its northern and southern margins (Girardeau *et al.* 1984; Yin & Harrison, 2000; Pan *et al.* 2004; Zhang *et al.* 2012). Moreover, many late Mesozoic intermediate–felsic magmatic rocks with ages ranging from 183 to 101 Ma are widely distributed in the southern QT (e.g. Kapp *et al.* 2005; Chang *et al.* 2011; Li *et al.* 2014*a*, *b*, 2016; Hao *et al.* 2016*a*, *b*; Zhu *et al.* 2016; Wei *et al.* 2017, 2018; Song *et al.* 2021).

The study area in this paper, the Rena-Co area (RCA), is located approximately 50 km northeast of Gerze County, Tibet, on the southern margin of the QT (Fig. 1b). The main strata exposed in the RCA are the middle Permian Longge Formation (P_2l), Upper Triassic Riganpeicuo Formation (T_3r), Lower-Middle Jurassic Sewa Formation ($J_{1\text{-}2}s$), Lower Cretaceous MF (K_1m) and Quaternary units. P_2l is mainly composed of microcrystalline limestone and fine-grained limestone. T_3r consists mainly of micritic limestone and bioclastic limestone. $J_{1\text{-}2}s$ is a complex unit of thinly bedded sandstone, medium-bedded quartzose sandstone, quartzofeldspathic sandstone and thinly bedded argillaceous slate. Notably, K_1m within the area of interest contains MF volcanic rocks, which are mainly dacite with minor andesite and rhyolite. In addition, this area contains several groups of faults and inferred faults across the basin, including NE–SW-trending, E–W-trending and nearly N–S-trending faults and/or inferred faults. The RCA contains several Mesozoic intermediate–silicic intrusions, including granodiorites, diorites and granodiorite porphyries (Fig. 1b).

The K_1m volcanic rocks are exposed mainly in the southern RCA. K_1m overlies $J_{1\text{-}2}s$ and T_3r across a buried angular unconformity. Our dacite samples analysed in this study were collected from K_1m west of the Rena-Co area in the southern QT, approximately 35 km north of the BNSZ (Fig. 1b). Petrographically, although our analysed volcanic rocks in the RCA are extensively altered, the original textures appear to have been preserved. The analysed dacites in this study have a porphyritic texture, containing 20–35 vol.% phenocrysts of plagioclase (15–20 vol.%), amphibole (5–10 vol.%) and pyroxene (3–5 vol.%). The matrix is mainly oriented or interleaved plagioclase microlites, cryptocrystalline, Fe–Ti oxides and minor quartz (Fig. 2).

3. Results

Analytical methods, whole-rock major and trace elements, Sr-Nd-Pb isotopes and LA–ICP–MS zircon U-Pb and Lu-Hf isotope data for the RCA volcanic rocks are given in Supporting Information I. Herein, we selected the least altered samples for geochemical and isotopic analyses, with their results presented in Supporting Information II.

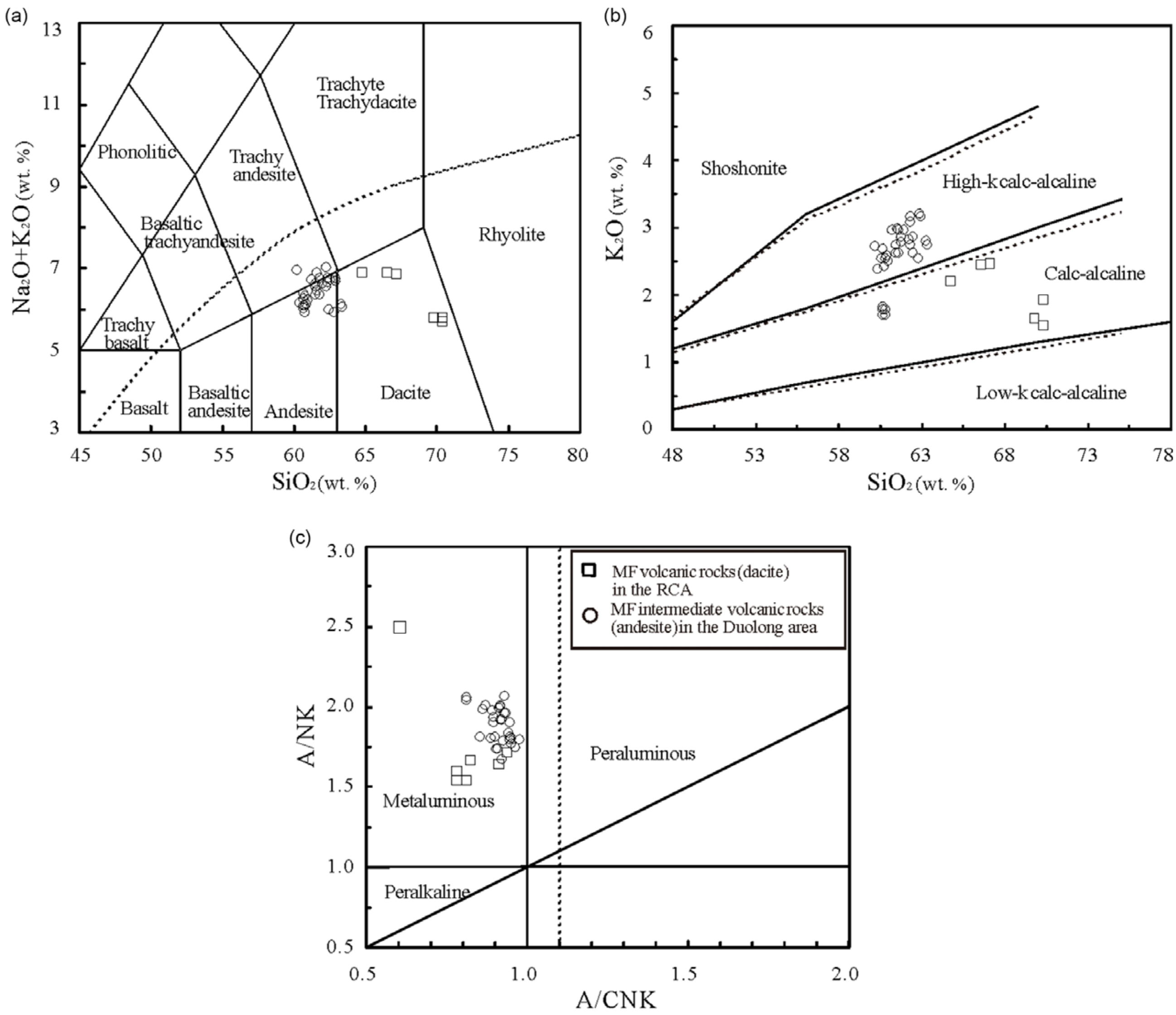

Figure 3. (Colour online) Selected plots of the MF volcanic rocks in the western QT, central Tibet. (a) Total alkalis (wt.%) vs. SiO_2 (wt.%) diagram (Middlemost, 1994) for classification, (b) K_2O (wt.%) vs. SiO_2 (wt.%) diagram (Peccerillo & Taylor, 1976), (c) A/NK vs. A/CNK diagram (Maniar & Piccoli, 1989). Analytical data of 33 other Duolong volcanic rocks samples collected from (Wang *et al*. 2015; Sun, 2015; Li *et al*. 2016; Wei *et al*. 2017; Shi *et al*. 2019) are shown for debate. See text for details.

3.1. Major and trace elements

Whole-rock major and trace element data for the RCA volcanic rocks are presented in Table A of Supporting Information II. Based on field and petrographic observations and loss on ignition (LOI) geochemical data in the analysed samples (1.62–4.44%), with an average of 3.03 wt.%, the analysed dacite samples are relatively fresh. When normalized on a volatile-free basis, the analysed dacite samples in this study are characterized by low TiO_2 contents (0.50–0.59 wt.%), low MgO contents (0.68–0.88 wt.%), low TFe_2O_3 contents (3.97–4.65 wt.%), low $Mg^{\#}$ values (23.83–29.65), as well as relatively high SiO_2 (64.79–70.37 wt.%), Na_2O (3.79–4.70 wt.%), K_2O (1.54–2.46 wt.%) and Al_2O_3 (13.81–16.13 wt.%) contents. The RCA dacite samples plot in the subalkaline dacite field in the SiO_2 vs. Na_2O + K_2O diagram (Fig. 3a) and in the medium-K calc-alkaline series in the K_2O vs. SiO_2 diagram (Fig. 3b), with total alkalis and K_2O/Na_2O ratios ranging from 5.71 to 6.91 and 0.36 to 0.56, respectively. Moreover, these samples share metaluminous characteristics, with A/CNK values (molar $Al_2O_3/[CaO+K_2O+Na_2O]$) of 0.78–0.94 (Fig. 3c).

These analysed rocks show a remarkably right deviation in the chondrite-normalized rare earth element (REE) patterns (Fig. 4a), with very low total REE contents (ΣREE = 98.8–123.1 ppm) and varying enriched light rare earth elements (La_N/Yb_N = 18.48–20.23, where N denotes values normalized to the chondrite composition of Sun & McDonough, 1989). They share slightly negative to negligible Ce anomalies [$\delta Ce = 0.89–1.01$, $\delta Ce = 2 \times Ce_N/(La_N+Pr_N)$] and weakly negative Eu anomalies [$\delta Eu = 0.84–0.89$, $\delta Eu = 2 \times Eu_N/(Sm_N+Gd_N)$]. They exhibit high Sr (517-598 ppm) and low Y (8.45-10.7 ppm) contents, coupled with limited Sr/Y ratios (11.0–13.7). In addition, they generally show strong enrichments in large ion lithophile elements (LILEs: K, Rb, U and Pb) relative to high-field-strength elements (HFSEs: Nb, Ta, and Ti) in primitive-mantle-normalized multielement

https://doi.org/10.1017/S0016756823000274 Published online by Cambridge University Press

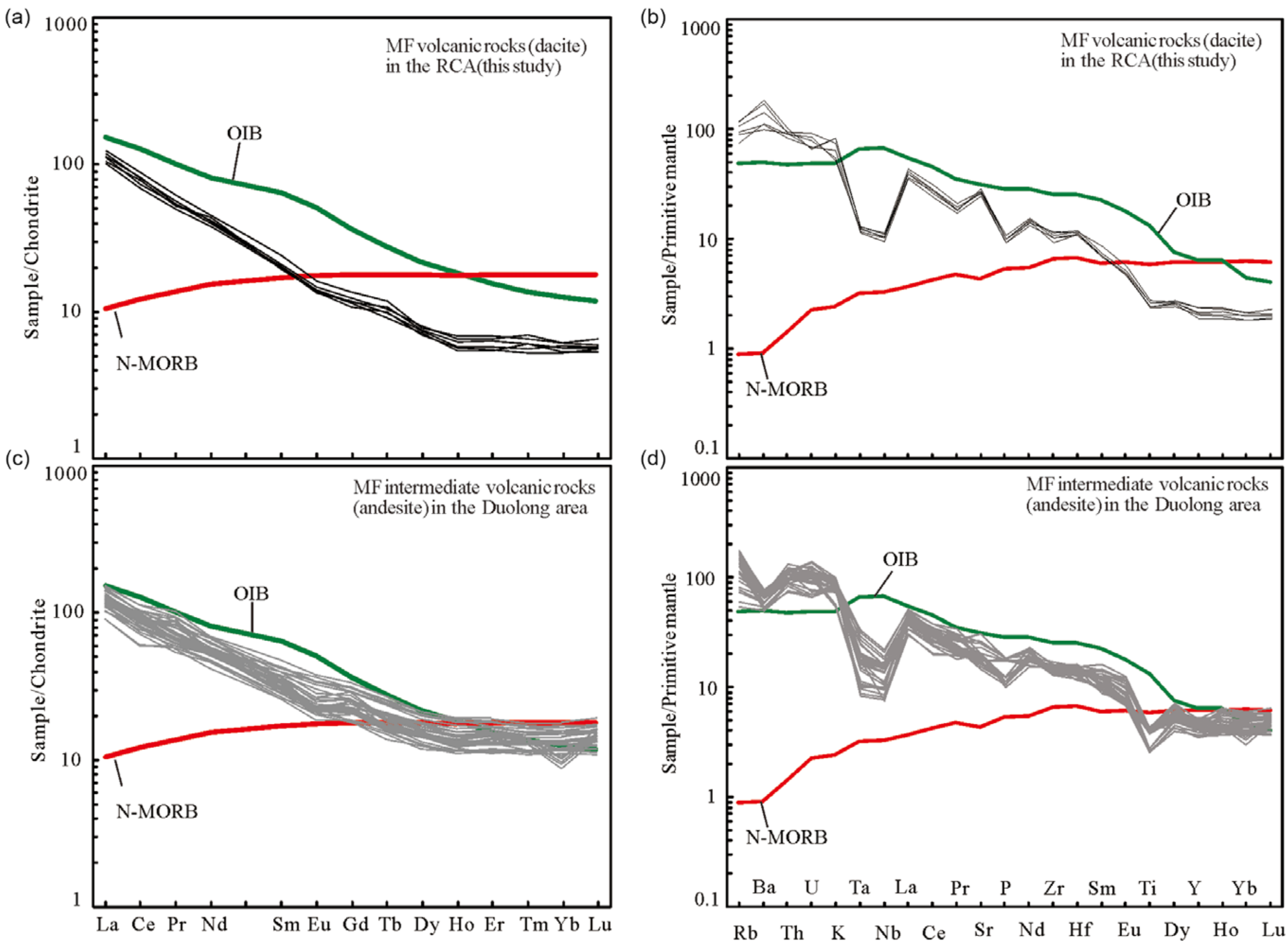

Figure 4. (Colour online) Chondrite-normalized REE (a, c, e) and primitive-mantle-normalized trace element patterns (b, d, f) for the MF volcanic rocks in the western QT, central Tibet. The date sources are for the MF volcanic rocks the same as in Figure 3. N-MORB and OIB (Sun & McDonough, 1989). Data for normalization and plotting are from Sun & McDonough (1989). Note that the MF volcanic rocks show significantly different patterns from those of N-MORB and OIB.

variation patterns (Fig. 4b), which are similar to the geochemical characteristics of arc-type magmas worldwide (Pearce & Peate, 1995; Wilson, 1989; Hawkesworth *et al.* 1993).

3.2. Zircon U-Pb ages

The zircon U-Pb dating results are listed in Table B of Supporting Information II. In cathodoluminescence (CL) images, zircons from the studied samples are mostly euhedral to subhedral in morphology. Zircons from sample RNC1610 have long axes of 50 µm to 220 µm and length-to-width ratios of 2:1 to 3:1 (Fig. 5a), while zircons from sample RNC1613 have long axes of 50 to 150 µm as well as length-to-width ratios of 1:1 to 3:1 (Fig. 5b). The CL images show that the zircon grains from these two samples have wide magmatic oscillatory zoning. The Th/U ratios of zircons range from 0.50 to 1.17 in sample RNC1610 and from 0.47 to 1.18 in sample RNC1613. Their generally high Th/U ratios, more than 0.1, indicate a magmatic origin (Corfu *et al.* 2003; Hoskin & Schaltegger, 2003). Thus, zircon U-Pb ages could be interpreted as representing the eruptive age of host rocks.

After rejecting discordant ages, the 21 analyses from sample RNC1610 are generally concordant and share zircon $^{206}Pb/^{238}Pb$ ages ranging from 108.8 Ma to 110.6 Ma (Fig. 5a), with a weighted mean age of 109.5±0.6 Ma (MSWD=0.02). Similarly, the 12 analyses from sample RNC1613 are also concordant and share zircon $^{206}Pb/^{238}Pb$ ages ranging from 108.3 to 110.8 Ma (Fig. 5b), with a weighted mean age of 109.6±0.8 Ma (MSWD= 0.01). Therefore, the RCA volcanic rocks were generated in the Early Cretaceous (ca. 109.5-109.6 Ma), similar to the Duolong MF volcanic rocks (105.7-118.5 Ma; Wang *et al.* 2015; Sun, 2015; Li *et al.* 2016; Wei *et al.* 2017; Shi *et al.* 2019) and the northern Gerze andesites (~124 Ma; Liu *et al.* 2012).

3.3. Whole-rock Sr-Nd-Pb isotopic data

Whole-rock Sr-Nd-Pb isotopic data are listed in Table C of Supporting Information II. All samples show homogeneous Sr-Nd-Pb isotopic compositions (Fig. 6). Initial Sr, Nd and Pb isotopic ratios were corrected by the ages of 109.5 Ma and 109.6 Ma. These dacite samples have low $^{87}Sr/^{86}Sr_{(i)}$ values (0.705119–0.705491) and exhibit a restricted range of $\epsilon_{Nd}(t)$ values ranging from −0.28 to +1.25 (corrected to related $^{206}Pb/^{238}U$ ages), with young single-stage Nd-depleted mantle ages of TDM1 = 642 to 818 Ma. In addition, these rocks exhibit variable $(^{206}Pb/^{204}Pb)_i$ values of 18.489 to 18.508, $(^{207}Pb/^{204}Pb)_i$ values of 15.591 to 15.612 and $(^{208}Pb/^{204}Pb)_i$ values of 38.599 to 38.686.

https://doi.org/10.1017/S0016756823000274 Published online by Cambridge University Press

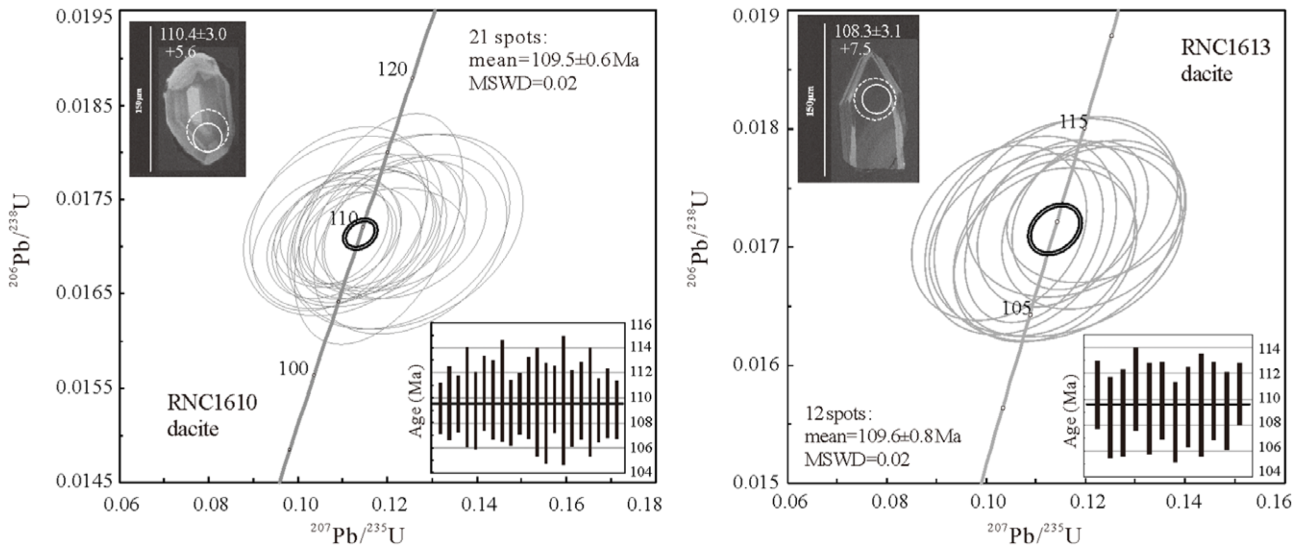

Figure 5. (Colour online) Cathodoluminescence (CL) images of representative zircon grains and concordia plots of the MF volcanic rocks in the RCA. Solid and dashed circles indicate the locations of LA-ICP-MS U-Pb dating and Hf analyses, respectively. The scale bar length in CL image is 150μm.

3.4. Zircon Hf isotopes

A total of 33 dated zircons were analysed by LA–MC–ICP–MS for Hf isotopes in this study, and the results of the initial $^{176}Hf/^{177}Hf_{(i)}$ ratios and $\epsilon_{Hf}(t)$ values are presented in Table D of Supporting Information II. These two analysed dacite samples share highly similar variations in Hf isotopes in zircons. Zircons from these dacites have uniform Hf isotopic compositions ($^{176}Hf/^{177}Hf_{(i)} = 0.282813$ to 0.283074), yielding $\epsilon_{Hf}(t)$ values and young Hf-depleted mantle ages (T_{DMC}) of +3.9 to +13.1 and 331 to 923 Ma (Fig. 7), respectively.

4. Discussion

4.1. Tectonic setting

The dacite samples, with ages of ca. 109.5–109.6 Ma, show remarkable enrichments in light REEs ($La_N/Yb_N = 18.48–20.23$) and LILEs (e.g. Cs, Rb, U, Pb and K) but significant depletions in HFSEs (e.g. Nb, Ta and Ti), consistent with the characteristics of arc-type volcanic rocks formed in a subduction zone environment (Fig. 4a, b; Hawkesworth *et al.* 1993; Pearce & Peate, 1995). In addition, they share similar geochemical signatures to the Early Cretaceous arc-type rocks related to the northern subduction of the Bangong–Nujiang oceanic lithosphere (BNOL), such as andesites from northern Gerze (ca. ~124 Ma, Liu *et al.* 2012), Duolong MF volcanic rocks with ages of ca. 105.7–118.5 Ma (Fig. 4c, d; Wang *et al.* 2015; Sun, 2015; Li *et al.* 2016; Wei *et al.* 2017; Shi *et al.* 2019) and Duolong ore-bearing and barren porphyry with ages of ca. ~116–128 Ma (e.g. She *et al.* 2009; Chen *et al.* 2013; Li *et al.* 2013*a*, 2016; Sun, 2015; Zhu *et al.* 2015; Wei *et al.* 2018). Note that the interval between the RCA and Duolong area measures only approximately 65 kilometres spatially, forming a nearly W-S magmatic belt parallel to the BNSZ (Fig. 1). In particular, the MF volcanic rocks from the two sections yield nearly identical ages, considering their error ranges, and have essentially identical REE and trace element patterns (Fig. 4a, b; Kapp *et al.* 2005; Chang *et al.* 2011; Wang *et al.* 2015; Sun, 2015; Li *et al.* 2016; Wei *et al.* 2017; Shi *et al.* 2019; this study). Taken together, these observations show that these two sections probably share the same tectonic setting.

Interpreting the tectonic setting of altered rocks is difficult. The chemistry of some elements, particularly LILEs (e.g. K, Ba, Rb and Sr), has been easily affected by alteration, whereas elements such as Ti, V, Zr, Hf, Nb, Ta, Y, Yb and La are effectively immobile during alteration (Allègre & Minster, 1978; Collins *et al.* 1982). Therefore, the latter immobile elements should be used in interpreting the tectonic setting of the RCA dacites. When plotted on a discrimination diagram using immobile minor and trace elements, all the MF volcanic rocks from the RCA, together with those from the Duolong area, plot in the arc volcanic setting field on the Hf/3-Th-Nb/16 diagram (Fig. 8a, Wood, 1980); this discrimination diagram could apply to both intermediate–acid rocks and basaltic rocks and is very useful for discriminating arc-related volcanic rocks (Wood *et al.* 1980; Hugh, 1993). Furthermore, the dacite samples share Ta/Yb ratios of 0.50–0.54, Nb/Yb ratios of 7.35–8.14 and Th/Yb ratios of 7.53–8.59, which plot within or near the active continental margin field rather than the within-plate field (including continental rifts and ocean islands) on the Th/Yb vs. Nb/Yb and Th/Yb vs. Ta/Yb diagrams (Fig. 8b, c; Pearce & Peate, 1995; Agrawal *et al.* 2008). Note that this is similar to the Andean arc basalts (continental island arc basalts). The Zr/Y ratios (11.02–13.70) of the RCA dacites are higher than the value of 3.0 that was used to separate the oceanic arc (Zr/Y < 3) and continental volcanic rocks (Zr/Y > 3; Pearce, 1982; Pearce *et al.* 1984; Pearce & Deng, 1988), indicating that the RCA dacites were most likely constructed in a continental island arc setting. Moreover, they share high La/Nb ratios ranging from 3.41 to 3.79 and negative Eu anomalies ranging from 0.84 to 0.89, all of which further reinforce the subduction-related tectonic setting (Condie, 2001). This view is also supported by the fact that these RCA volcanic rocks have high SiO_2 (64.79–70.37 wt.%) and moderate K_2O (1.54–2.46 wt.%) contents, with all the samples plotting in the medium-K calc-alkaline series field (Fig. 3b), given that calc-alkaline volcanic rocks have long been considered the result of subduction-related arc magmatism occurring at convergent plate boundaries (e.g. Li *et al.* 2013*b*, 2015; and references therein).

Hence, as presented above, the geochemical features clearly suggest that the MF dacites from the RCA possess an arc volcanic signature that corresponds with subduction, likely suggesting that

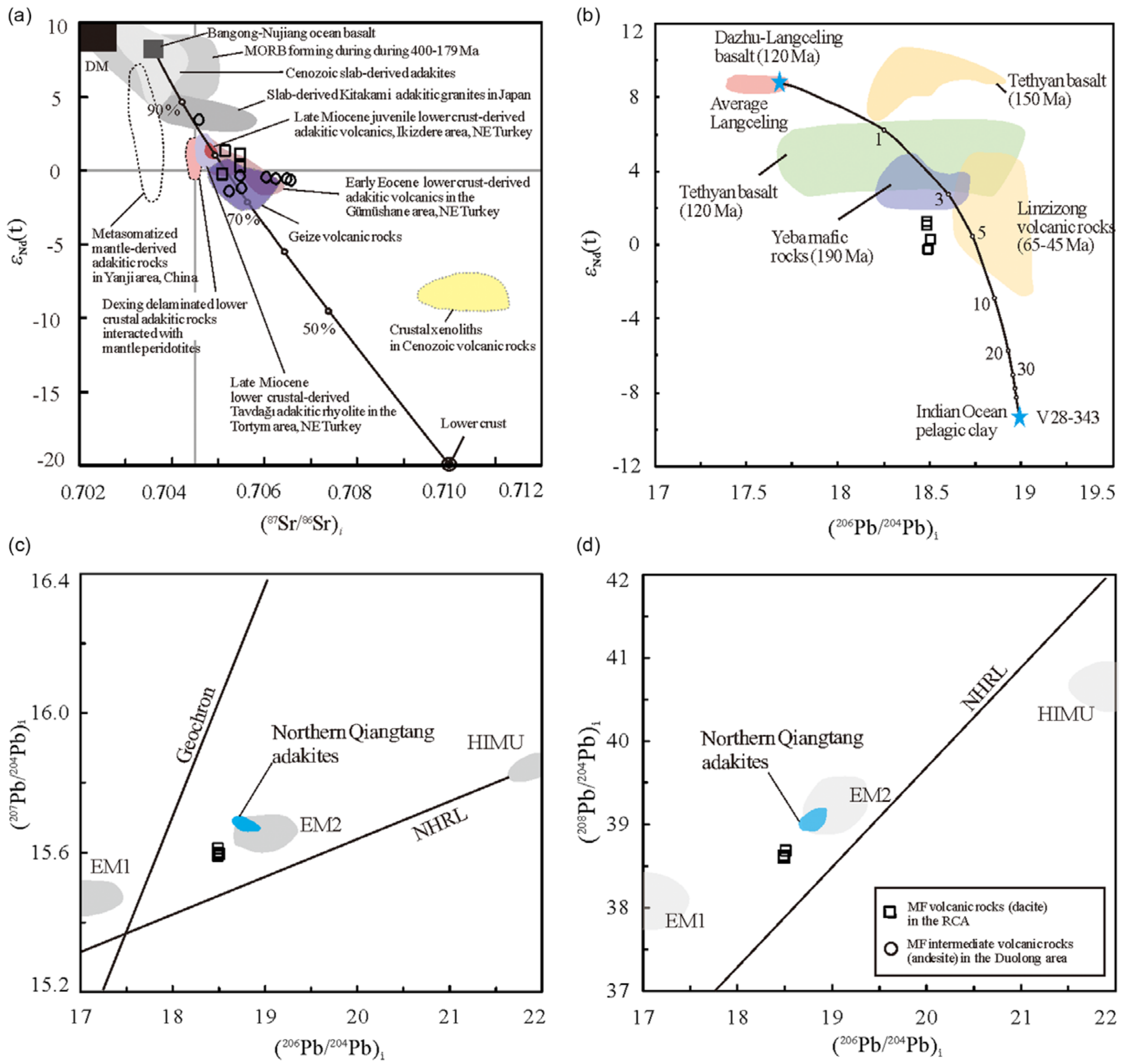

Figure 6. (Colour online) Whole-rock Sr, Nd and Pb isotopic compositions of the MF volcanic rocks in the western QT, central Tibet. Analytical Sr and Nd isotopic data of 12 Duolong volcanic rocks samples collected from previous studies (Sun, 2015; Li *et al*. 2016; Wei *et al*. 2017) are shown for debate. In Panel a, data of Bangong–Nujiang Ocean basalt (Liu *et al*. 2014), MORB forming during 400-179 Ma (Hofmann, 2003), the lower crust (Miller *et al*. 1999), crustal xenoliths in Cenozoic volcanic rocks (Lai & Qin, 2008), Dexing lower crustal derived adakitic rocks (Wang *et al.* 2006*b*),Cenozoic slab-derived adakites (Defant & Kepezhinskas, 2001), the Gerze volcanic rocks (Liu *et al*. 2012), Slab-derived adakites in Kitakami area and Metasomatized mantle-derived adakites in Yanji area (Tsuchiya *et al*. 2005), Early Eocene lower crust-derived adakitic rocks in Gümüşhane area (Karsli *et al*. 2010), Late Miocene mafic lower crust-derived Tavdağı adakites in the Tortum area (Dokuz *et al*. 2013) and Late Miocene juvenile lower crust-derived adakites in IKizdere area (Karsli *et al*. 2019) are shown for comparison. In Panel b, data of Tethyan basalts (150 Ma and 120 Ma; Mahoney *et al*. 1998), Dazhu-Langceling basalts from the Yarlung Zangbo suture zone (Zhang *et al*. 2005), Indian Ocean pelagic sediment (V28-343, Ben Othman *et al*. 1989), Yeba mafic rocks (Zhu *et al*. 2008), and Linzizong andesites (Mo *et al*. 2006, 2007) are shown for comparison. The star at the top in Panel b is the average value for Langceling basalts (Zhang *et al*. 2005), and Indian Ocean pelagic sediment is used as a proxy for oceanic sediment. In Panel c and d, NHRL is from Hart (1984), Geochron (4.55 Ga) and the mantle end-members HIMU, EM1 and EM2 are after Zindler & Hart (1986), and Northern Qiangtang adakitic rocks are from Lai *et al*. (2007). See text for details.

they formed at a continental margin arc due to the northwards subduction of the BNOL.

4.2. Petrogenesis of the RCA dacites

As outlined above, our MF dacites from the RCA in this study contain plagioclase phenocrysts are characterized by relatively high SiO_2 abundances (64.79–70.37 wt.%), high Al_2O_3 abundances (13.81–16.13 wt.%), high Na_2O abundances (3.79–4.70 wt.%) and high Sr abundances (517-598 ppm), but low Y abundances (8.45-10.7 ppm), low Yb abundances (0.89-1.04 ppm), low Cr abundances (33.3-58.9 ppm) and low Ni abundances (17.6-33.6 ppm), with limited Sr/Y ratios of 11.0–13.7 and La_N/Yb_N ratios of 18.48–20.23, and they plot within the adakite field of Figure 9a. In addition, they yield weakly negative to positive whole-rock $\epsilon_{Nd}(t)$ values (−0.28 to +1.25) and positive zircon $\epsilon_{Hf}(t)$ values (+3.9 to +13.1). Overall, the RCA dacites display adakite-like geochemical characteristics (Fig. 9a,

https://doi.org/10.1017/S0016756823000274 Published online by Cambridge University Press

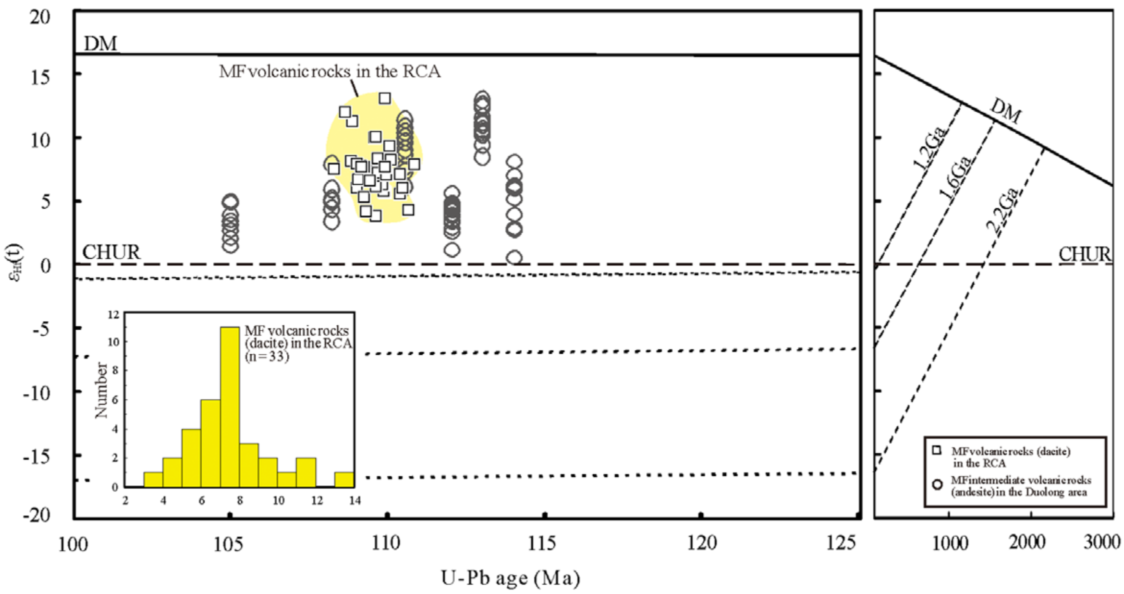

Figure 7. (Colour online) Zircon $\epsilon_{Hf}(t)$ vs. U-Pb ages diagram of the MF volcanic rocks in the western QT, central Tibet. Analytical data of 6 Duolong volcanic rocks samples collected from previous studies (Sun, 2015; Li *et al.* 2016; Wei *et al.* 2017) are shown for debate. Inset in the diagram shows histograms of $\epsilon_{Hf}(t)$ zircons of the MF volcanic rocks from the RCA.

Defant & Drummond, 1990). Thus far, several hypotheses have been proposed to explain the origin of adakitic rocks, including (a) melting of subducted young and hot oceanic slabs (e.g. Stern & Kilian, 1996; Defant & Drummond, 1990; Rapp *et al.* 1999; Defant *et al.* 2002); (b) assimilation fractional crystallization (AFC) or fractional crystallization (FC) from parental basaltic magmas (e.g. Feeley & Hacker, 1995; Castillo *et al.* 1999; Macpherson *et al.* 2006); (c) magma mixing between felsic and basaltic magmas (e.g. Streck *et al.* 2007); (d) melting of delaminated lower crust (e.g. Kay & Kay, 1993; Xu *et al.* 2002; Gao *et al.* 2004; Wang *et al.* 2006*a*, *b*); and (e) melting of thickened mafic lower continental crust (e.g. Atherton & Petford, 1993; Hou *et al.* 2004; Chung *et al.* 2003, 2005).

We argue that the first four genetic hypotheses are not applicable to the RCA dacites based on the following observations. First, adakites from modern arcs that are interpreted as slab melts have mid-ocean-ridge basalt (MORB)-like Sr–Nd isotopic compositions and relatively low K_2O, Th and Th/La values, which originate from the basaltic portion of subducting slabs (Defant & Drummond, 1990; Kelemen *et al.* 2003; Plank, 2005). In the case of the studied adakite-like dacites from the RCA, they have more evolved Sr-Nd-Pb isotopic compositions (Fig. 6) and much higher K_2O contents (1.54–2.46 wt.%), with K_2O/Na_2O ratios of 0.36–0.56, as well as varying higher Th values (6.9-8.6 ppm) and Th/La ratios (0.27–0.32) than those of the MORB and slab-derived (subducted oceanic crust-derived) adakites (Fig. 9c; e.g. Niu & Batiza, 1997; Martin *et al.* 2005; Wang *et al.* 2008*a*, *b*; Tang *et al.* 2010). They are geochemically distinct from the Hohxil adakites produced by melting of subducted sediments on the northwards-subducting Songpan–Ganzi oceanic slab (Fig. 9c; Wang *et al.* 2005, 2008*a*) and the Mamen adakite-like rocks derived from partial melting of the subducted oceanic slab (MORB + sediment + fluid) (Zhu *et al.* 2009). On the other hand, if the dacites originated as subducted slab melts, they should have mid-ocean-ridge basalt-like Sr–Nd isotopic compositions ($\epsilon_{Nd}(t)\approx10$; Defant & Drummond, 1990), as shown by the Bangong–Nujiang oceanic basalt (Fig. 6a; Zhu *et al.* 2006; Liu *et al.* 2014). As shown in Fig. 6a, the RCA adakite-like dacites show a more radiogenic Sr–Nd isotope signature than MORB that formed at 400-179 Ma (Hofmann, 2003), Cenozoic adakites that formed in a subducting environment (e.g. Kimura *et al.* 2014), adakites that formed by the partial fusion of modified lithospheric mantle in the Yanji region (Guo *et al.* 2007) and adakites that originated from slab-derived melt in the Kitakami region (Tsuchiya *et al.* 2005). In addition, their features of negative Nb–Ti anomalies are not consistent with N-MORB, OIB or oceanic slab sources resulting in melts, as identified by positive Nb–Ti anomalies in the spidergrams normalized to the primitive mantle (Fig. 4a, b; e.g. Sun & McDonough, 1989; Hofmann, 1997), suggesting that their source rocks were not basaltic oceanic crust.

Second, suites of adakitic rocks derived by fractional crystallization of basaltic magmas usually exhibit variable and high Gd/Yb ratios in addition to high La/Yb and Sr/Y ratios (Macpherson *et al.* 2006; Richards & Kerrich, 2007). However, the RCA dacites exhibit low and relatively low Gd/Yb ratios (2.43–2.67), with low La/Yb ratios of 25.8 to 28.2 and Sr/Y ratios of 53.0 to 70.8. Geochemically, adakites generated by this process generally display distinct compositional trends, in which the Al_2O_3 and La contents decrease with increasing SiO_2 contents, but the La/Y, Dy/Yb and Sr/Y ratios clearly increase with increasing SiO_2 contents (Macpherson *et al.* 2006). Nevertheless, the RCA dacites obviously exhibit none of these trends, with a relatively narrow range of SiO_2 contents (64.79–70.37 wt.%). In other words, fractional crystallization can also be ruled out because of the lack of a negative linear correlation between SiO_2 concentrations and $Mg^{\#}$ values (Fig. 9b; Castillo *et al.* 1999), as well as a lack of a positive linear correlation between SiO_2 concentrations and Sr/Y and $(Dy/Yb)_N$ values (not shown; Macpherson *et al.* 2006), for the RCA adakite-like dacites. Furthermore, these adakite-like dacites are not associated with contemporary basaltic rocks that would correspond to the required mafic end-member in AFC, FC and magma mixing models (e.g. Castillo *et al.* 1999; Macpherson *et al.* 2006; Streck *et al.* 2007), indicating that they could not have been generated directly by crustal assimilation and fractional crystallization from parental basaltic magmas.

https://doi.org/10.1017/S0016756823000274 Published online by Cambridge University Press

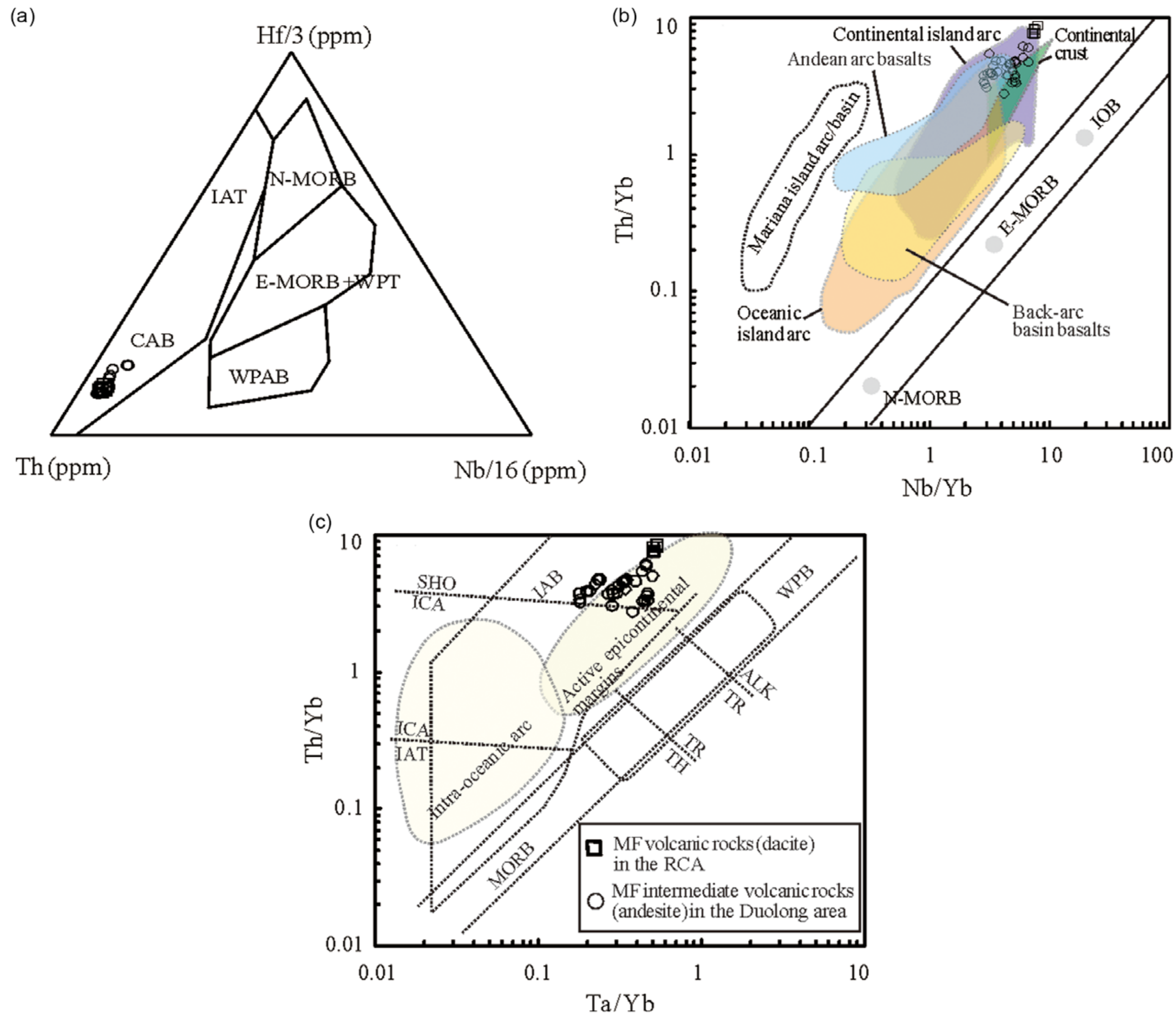

Figure 8. (Colour online) Selected discrimination diagrams of the MF volcanic rocks in the western QT, central Tibet. (a) Th/Yb-Ta/Yb diagrams (Pearce, 1982); (b) Th/Yb-Nb/Yb diagrams (Pearce & Peate, 1995); (c) Hf/3-Th-Nb/16 diagram (Wood, 1980). The date sources for the MF volcanic rocks are the same as in Figure 3. Note that the MF volcanic rocks were formed in a continental margin setting.

Third, it appears unlikely that they formed as a product of magma mixing between felsic and basaltic magmas, as they contain no mafic microgranular enclaves, as also evidenced by the lack of straight linear variations between the concentrations of major elements, such as MgO, K_2O, Al_2O_3 and SiO_2, within these rocks. Moreover, these samples show weakly negative to positive whole-rock $\epsilon_{Nd}(t)$ values (Fig. 6a, b; −0.28 to +1.25) and positive zircon $\epsilon_{Hf}(t)$ values (Fig. 7; +3.9 to +13.1), which are inconsistent with formation from magma mixing between felsic and basaltic magmas.

Fourth, their formation was not related to melting of delaminated lower crust. These RCA adakite-like dacites have whole-rock radiogenic Sr isotope [$^{87}Sr/^{86}Sr_{(i)} = 0.705119–0.705491$], Nd isotope [$\epsilon_{Nd}(t)$ of −0.28 to +1.25] and Pb isotope [$(^{206}Pb/^{204}Pb)_i = 18.489–18.508$, $(^{207}Pb/^{204}Pb)_i = 15.591–15.612$, $(^{208}Pb/^{204}Pb)_i = 38.599–38.686$] compositions (Fig. 6b, c, d), which are remarkably different from the crustal xenoliths in Cenozoic volcanic rocks from the QT, northern Tibet (Fig. 6a; Lai & Qin, 2008). As mentioned above, their geochemical and Sr–Nd isotopic features significantly differ from those of the Cenozoic crust-derived adakites of the Songpan–Ganzi block (Fig. 6c, d; Wang *et al.* 2008*a*), the Mesozoic Anjishan adakites from the Ningzhen area of East China generated by partial melting of delaminated lower continental crust [$\epsilon_{Nd}(t) = −6.8$ to $−9.7$, $(^{87}Sr/^{86}Sr)_i = 0.7053$ to 0.7066, Xu *et al.* 2002], the Zougouyouchaco and Dogai Coring adakitic volcanic rocks in the southern and middle Qiangtang region that were most likely derived from partial melting of delaminated lower continental crust [$\epsilon_{Nd}(t) = −3.8$ to $−5.0$, $(^{87}Sr/^{86}Sr)_i = 0.706–0.708$; Liu *et al.* 2008], and the Dexing adakites originating from the partial fusion of delaminated lower crust that experienced a melt and mantle peridotite interaction (Wang *et al.* 2006*b*). Moreover, their low $Mg^{\#}$ values (23.83–29.65) and low MgO abundances (0.68–0.88 wt.%) also argue against the origin of melting of delaminated lower crust (Fig. 9b).

We suggest that the RCA adakite-like dacite suites were probably generated by melting of juvenile mafic lower continental crust. Notably, their typical geochemical magmatic arc signatures, such as enrichment in LILEs, depletion in HFSEs, especially negative

https://doi.org/10.1017/S0016756823000274 Published online by Cambridge University Press

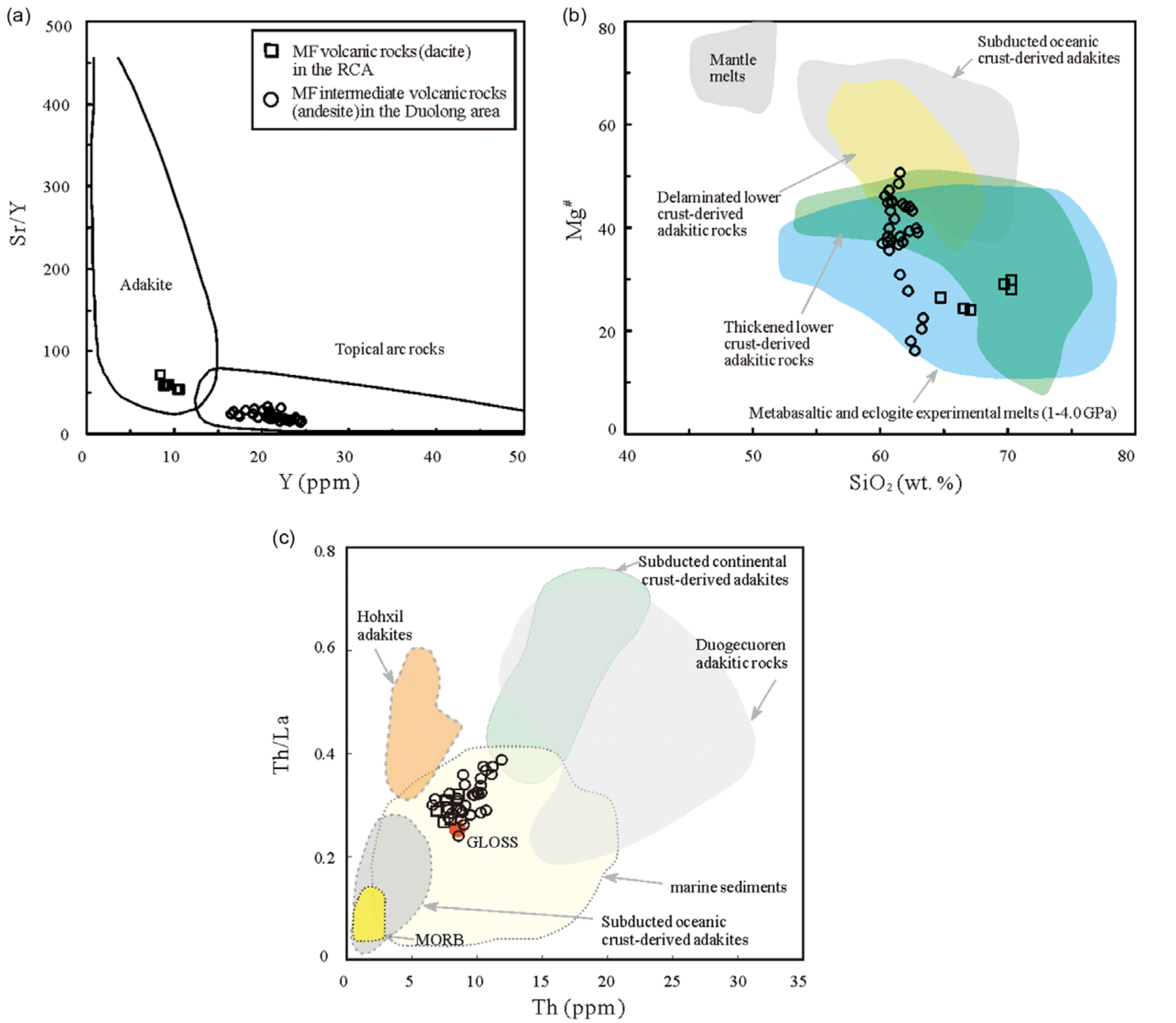

Figure 9. (Colour online) Selected discrimination diagrams of the MF volcanic rocks in the western QT, central Tibet. (a) Sr/Y vs. Y (ppm) diagram showing data for adakites and normal calc-alkaline rocks (Defant & Drummond, 1990), (b) $Mg^{\#}$ vs. SiO_2 (wt.%) diagram and (c) Th/La vs. Th (ppm) diagram (Plank, 2005). The date sources for the MF volcanic rocks are the same as in Figure 3. In Panel b, data of metabasaltic and eclogite experimental melts (1-4 Gpa) (Rapp *et al*. 1999, 2003, and references therein), subducting oceanic crust-derived adakites, delaminated lower crust-derived adakites and thickened lower crust-derived adakites (Wang *et al*. 2006*a*, *b*, 2008*a*, *b*, and references therein) are shown for debate. In Panel c, data of marine sediments and GLOSS (global subducting sediment) (Plank & Langmuir, 1998), MORB (Niu & Batiza, 1997), subducted oceanic crust-derived adakites (Defant *et al*. 2002; Martin *et al*. 2005), subducting continental crust-derived adakites (Wang *et al*. 2008*a*, *b*), Hohxil adakites (Wang *et al*. 2005, 2008*a*, *b*) and Duogecuoren adakitic rocks (Wang *et al*. 2005, 2008*a*, *b*) are shown for debate. See text for details.

Nb–Ta–Ti anomalies, and light REE (LREE)-enriched chondrite-normalized REE patterns ($La_N/Yb_N = 18.48–20.23$), with relatively negative Eu anomalies ($\delta Eu = 0.84–0.89$), are consistent with those of rhyolites in the Rena-Co area (ca. 110 Ma), which are proposed to be derived from juvenile crust (Chang *et al.* 2011). In particular, they show relatively low MgO and Mg# values and Cr and Ni contents, which are very comparable with those of adakitic rocks originating from the anatexis of the thickened lower crust (Castillo, 2012). Melting experiments of natural hydrous basalts under 0.8–3.2 GPa have revealed that pristine melts of basaltic rocks typically display low MgO and $Mg^{\#}$ values (generally lower than 43; Rapp & Watson, 1995). As mentioned earlier, the RCA adakite-like dacites yield low MgO and $Mg^{\#}$ values, similar to those of the pure experimental melts, which further confirms an origin of juvenile lower crustal melts for their generation (Fig. 9b; e.g. Rapp *et al.* 1999, 2003; Rapp & Watson, 1995).

They display low initial $^{87}Sr/^{86}Sr_{(i)}$ values of 0.705119 to 0.705491, weak negative to positive whole-rock $\epsilon_{Nd}(t)$ values of -0.28 to $+1.25$ and positive zircon $\epsilon_{Hf}(t)$ values from $+3.9$ to $+13.1$, which are features that might have been inherited from juvenile crustal magmas. As shown in Figure 6a, the adakitic dacites have Sr–Nd isotope signatures identical to those of the late Miocene juvenile lower crust-derived adakitic volcanics in the Ikizdere area (Karsli *et al.* 2019), the late Miocene mafic lower crust-derived Tavdağı adakitic rhyolite in the Tortum area (Dokuz *et al.* 2013) and the early Eocene lower crust-derived adakitic volcanics in the Gümüşhane area (Karsli *et al.* 2010). Furthermore, the adakite-like dacites share relatively young

https://doi.org/10.1017/S0016756823000274 Published online by Cambridge University Press

T_{DM2} ages ranging from 806 to 931 Ma and Palaeozoic and Neoproterozoic Hf crustal model ages of 332 to 924 Ma, possibly suggesting that they were likely inherited from the melts of juvenile basaltic crust, which in turn was derived from old depleted mantle (van de Zedde & Wortel, 2001). This view is also supported by the fact that these samples have much more enriched whole-rock Sr–Nd isotopic compositions and more depleted zircon Hf isotopic compositions than those of the existing Jurassic intrusive rocks in the southern QT, such as the Larelaxin, Caima, Qingcaoshan, Charkang-Co and Rena-Co plutons, which are considered to be generated by partial melting of ancient lower continental crustal materials or by the mixing of crust-derived and mantle-derived melts (e.g. Li *et al.* 2014*a*, *b*; Hao *et al.* 2016*a*, *b*; and references therein).

Note that zircons from the RCA adakite-like dacite samples show large variations in their $\epsilon_{Hf}(t)$ values (up to 7.8 and 9.2 ϵ units for the two samples, respectively), thereby indicating an open magmatic system process (Griffin *et al.* 2002; Kemp *et al.* 2007; Chiu *et al.* 2009). This hypothesis is also supported by highly radiogenic Pb isotopic compositions between mantle and crust xenoliths (Fig. 6b, c, d; Lai & Qin, 2008), likely indicating a mixing trend. The $(^{207}Pb/^{204}Pb)_i$ values of 15.591–15.612 and $(^{208}Pb/^{204}Pb)_i$ values of 38.599–38.686 in the rocks are unusually radiogenic and plot well above the Northern Hemisphere Reference Line (NHRL) (Hart, 1984), shifting to higher $(^{206}Pb/^{204}Pb)_i$ values of 18.489–18.508 than the Geochron (4.55 Ga) (Fig. 6c, d). In addition, their $\epsilon_{Hf}(t)$ values (+3.9 to +13.1; n = 33) are similar to those of the Duolong Early Cretaceous volcanic rocks and intrusive rocks that are considered to be derived from juvenile lower crust (e.g. She *et al.* 2009; Xin *et al.* 2009; Chen *et al.* 2013; Li *et al.* 2013*a*, 2016; Sun 2015; Zhu *et al.* 2015; Wei *et al.* 2017, 2018). Notably, these volcanic rocks from the RCA show lower zircon $\epsilon_{Hf}(t)$ values than depleted mantle (Fig. 7), possibly implying at least partial contributions from metasomatized peridotite with partial melts of subduction-related fluids into their magma source (Woodhead *et al.* 2001; Barry *et al.* 2006). Such a foregoing interpretation is consistent with the modelling curves defined by the MF adakite-like rocks from the RCA in Sr–Nd and Nd–Pb isotope diagrams (Fig. 6a, b). Consequently, we consider that the RCA volcanic rocks contain a great proportion of approximately 75–80% mantle-derived material contributions, according to their Sr–Nd isotopic compositions (Fig. 6a), as well as melts of ~3–5% subduction-related fluids, according to their Nd–Pb isotopic compositions (Fig. 6b), given that a small contribution of fluids can sensitively cause a drastic increase in $^{206}Pb/^{204}Pb$ ratios in subduction-related rocks (Vroon *et al.* 1995; Rolland *et al.* 2002). In particular, the same observations occurred for igneous rocks of the Cretaceous Ladakh arc (Rolland *et al.* 2002) and the Cretaceous Kohistan island arc (Bignold & Treloar, 2003), of which several percent of subduction-related fluids became entrained into the magma source regions, in accordance with the measured Sr-Nd-Pb isotopic compositions.

In summary, these observations lead us to infer that the RCA adakite-like dacites were derived from melting of juvenile thickened mafic lower continental crust that contains melts of metasomatized peridotite and subduction-related fluids in the magma source region, likely as a result of the northern subduction of the BNOL beneath the southern QT.

4.3. Geodynamic implications

As one of the ancient orogens in the Tibetan Plateau, the BNSZ extending along central Tibet represents the oceanic remnant of the Bangong–Nujiang Tethyan Ocean (e.g. Allègre *et al.* 1984; Hsu *et al.* 1995; Pearce & Deng, 1988; Yin & Harrison, 2000; Kapp *et al.* 2003, 2005, 2007). Zhu *et al.* (2016) argued a model in which the Bangong Ocean may have closed through arc–arc 'soft' collision driven by divergent double-sided subduction rather than continent–continent 'hard' collision. Some studies have argued that the BNO closed between the Late Jurassic and the Early Cretaceous (Yin & Harrison 2000; Kapp *et al.* 2005; Sui *et al.* 2013; Wang *et al.* 2016; Zhu *et al.* 2016; Hu *et al.* 2022). However, numerous recent studies that have focused on radiolarians, ophiolitic fragments and mélanges within the BNSZ (Zhu *et al.* 2006; Bao *et al.* 2007; Baxter *et al.* 2009; Fan *et al.* 2014; Zhang *et al.* 2014) suggest that the BNO was still open during the Early Cretaceous and that the final Lhasa–Qiangtang amalgamation occurred in the Late Cretaceous (approximately 100 Ma; e.g. Baxter *et al.* 2009; Fan *et al.* 2014) rather than in the Late Jurassic–Early Cretaceous (e.g. Xu *et al.* 1985; Dewey *et al.* 1988; Yin *et al.* 1988; Kapp *et al.* 2003, 2005, 2007; Raterman *et al.* 2014), as also exemplified by the abundant Early Cretaceous magmatic rocks in the southern QT, which are interpreted as having formed in a continental arc setting (e.g. Kapp *et al.* 2005, 2007; Chang *et al.* 2011; Liu *et al.* 2012; Hao *et al.* 2016*a*, *b*; Wang *et al.* 2015; Sun, 2015; Li *et al.* 2013*a*, *b*, 2015, 2016; Wei *et al.* 2017, 2018; Shi *et al.* 2019; this study). Stratigraphic analysis suggests that the QT underwent N–S-directed compression and significant crustal shortening during the Early Cretaceous (Murphy *et al.* 1997; Kapp *et al.* 2005, 2007), probably as a result of the collision of an oceanic plateau with the Qiangtang continental margin (Zeng *et al.* 2021). It has long been recognized that the BNOL subducted northwards beneath the southern QT before the closure of the BNO (e.g. Allègre *et al.* 1984; Yin & Harrison, 2000; Guynn *et al.* 2006; Kapp *et al.* 2003, 2005, 2007; Zhu *et al.* 2016; Wei *et al.* 2018). Our data reveal the presence of adakite-like dacites with ages of 109.5–109.6 Ma in the RCA, approximately 30 km to the north of the BNSZ (Fig. 1b). These adakite-like dacites formed from magmas generated by melting of juvenile lower crustal material and have compositions consistent with adakites that formed in a continental marginal arc. Together with previous data on the Early Cretaceous intrusive and volcanic rocks (especially the Duolong Meriqiecuo volcanic rocks) distributed in the southern QT (She *et al.* 2009; Xin *et al.* 2009; Liu *et al.* 2012; Chen *et al.* 2013; Li *et al.* 2013*a*, 2016; Wang *et al.* 2015; Sun, 2015; Zhu *et al.* 2016; Wei *et al.* 2017, 2018; Shi *et al.* 2019), we confidently propose that the sources of the RCA adakite-like magmas were most likely associated with crustal thickening, given that crustal thickening is a common geological phenomenon in arc settings. All of this evidence indicates that the timing of the final closure of the BNO might have been later than the Early Cretaceous (109.5.9-109.6 Ma).

Recently, Hao *et al.* (2016*a*, *b*) also suggested that ancient lower crust was gradually replaced by younger materials between the Late Jurassic and Early Cretaceous and finally resulted in vertical crustal growth by magma underplating for the southern Qiangtang continental arc, based on the tracking of the magma sources of the late Mesozoic intermediate–felsic intrusive rocks in southern Qiangtang. Generally, such magma underplating is considered a result of asthenospheric upwelling, which is related to oceanic subduction with a slab rollback component due to drag and gravity forces (Nakakuki & Mura, 2013). As discussed above, the magma of the RCA adakite-like dacites most likely originated from melts of juvenile thickened lower crust. In this case, we suggest that a slab rollback model explains the magmatic flare-up that occurred in the

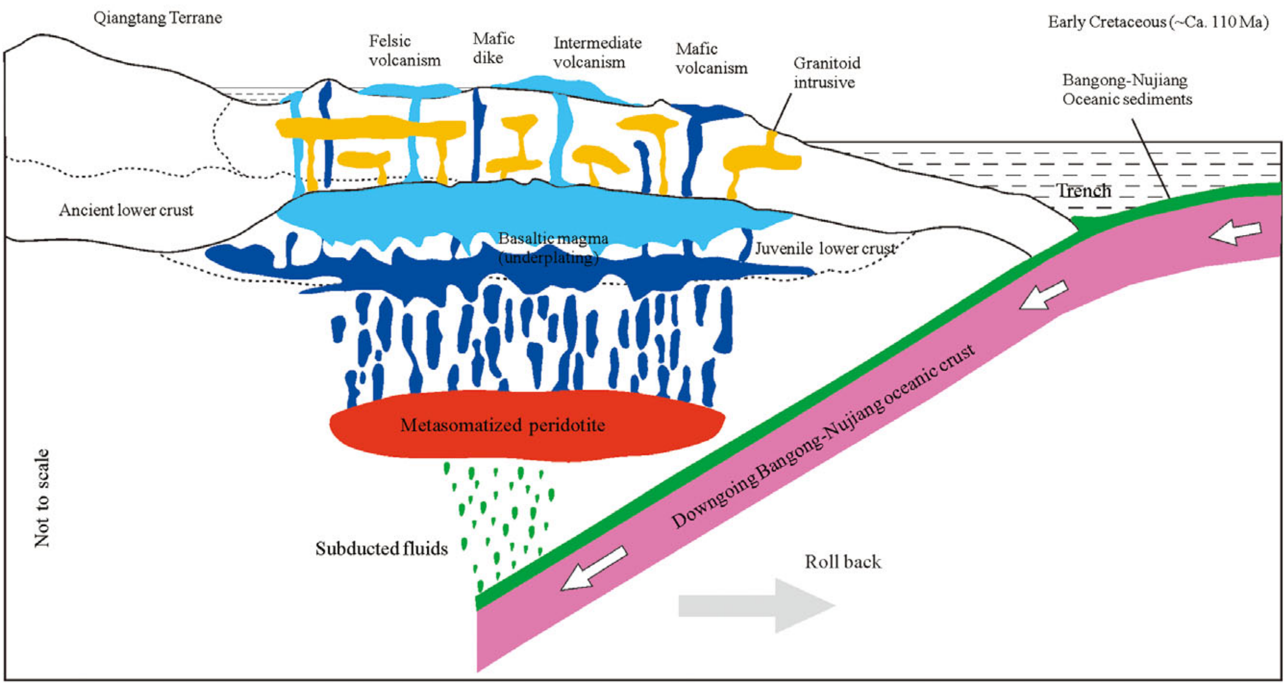

Figure 10. (Colour online) Schematic illustrations showing the geodynamic evolution of the Bangong–Nujiang oceanic northern subduction beneath QT during the Early Cretaceous (modified from Richards (2003) and Zhu *et al*. (2008)). Note that a slab rollback model combining Bangong–Nujiang oceanic subduction and underplating of mafic magmas proposed for the generation of the Early Cretaceous Meiriqiecuo magmatism in the southern QT. See text for details.

southern QT during the Early Cretaceous and accounts for the formation of the RCA adakite-like dacites (ca. 109.5-109.6 Ma). This mechanism may also apply to the geological processes in the northern Lhasa and Tethyan Himalayan thrust belts (Raterman *et al*. 2014; Zhu *et al*. 2016), both of which represent passive margins on the lower subducting plate of a collision zone.

In this model, the downgoing BNOL carried subducted fluids into the deep mantle during its northwards subduction and then resulted in the initiation of partial melting of mantle peridotite (Elliott *et al*. 1997). Subsequently, variable degrees of partial melts of mantle peridotite metasomatized by subducted fluids moved upwards, and basaltic underplating gradually replaced the ancient lower crust and accumulated to form juvenile basaltic crust. Thus, as a result of Early Cretaceous slab rollback, this newly underplated juvenile basaltic lower crust was further heated by a flow of upwelling hot asthenospheric materials (van de Zedde & Wortel, 2001; Zhu *et al*. 2016; Li *et al*. 2013*b*, 2015), finally leading to the generation of primary basaltic magmas for the RCA adakite-like dacites (Fig. 10; Richards, 2003; Zhu *et al*. 2008).

5. Conclusions

(1) Zircon U-Pb dating suggests that the RCA dacites formed at 109.5.9-109.6 Ma, marking Late Cretaceous volcanic magmatism during the northern subduction of the BNOL beneath the southern QT.
(2) They exhibit geochemical features with adakite affinity and most likely originated from melts of the juvenile continental lower crust, which contains melts of metasomatized peridotite and subduction-related fluids in the magma source region.
(3) Based on previous studies and our new data, we propose that a slab rollback model could explain the formation of the RCA adakite-like dacites, which was most likely associated with crustal thickening.

Supplementary material. To view supplementary material for this article, please visit https://doi.org/10.1017/S0016756823000274

Acknowledgements. This research was supported by Research grants from National Institute of Natural Hazards, Ministry of Emergency Management of China (Grant Number: ZDJ2019-01) and the Program of the China Geological Survey (Grant Number: DD20190167). We thank the laboratorians for helping with zircon U-Pb age and Lu-Hf isotopic, whole-rock geochemical and Sr-Nd-Pb isotopic analysis. Besides, we also thank two anonymous reviewers for their constructive reviews that improved the quality of this manuscript.

Declaration of Competing Interest. The authors declare that they have no known competing financial interests or personal relationships that could have appeared to influence the work reported in this paper.

References

Agrawal S, Guevara M and Verma SP (2008) Tectonic discrimination of basic and ultrabasic rocks through log-transformed ratios of immobile trace elements. *International Geology Review* **50**, 1057–79.

Allègre CJ, Courtillot V, Tapponnier P, Hirn A, Mattauer M, Coulon C, Jaeger JJ, Achache J, Schärer U, Marcoux J, Burg JP, Girardeau J, Armijo R, Gariépy C, Göpel C, Li TD, Xiao XC, Chang CF, Li GQ, Lin BY, Teng JW, Wang NW, Chen GM, Han TL, Wang XB, Den WM, Sheng HB, Cao YG, Zhou J, Qiu HR, Bao PS, Wang SC, Wang BX, Zhou YX and Xu RH (1984) Structure and evolution of the Himalaya-Tibet orogenic belt. *Nature* **307**, 17–22.

Allègre CJ and Minster JF (1978) Quantitative models of trace element behavior in magmatic processes. *Earth and Planetary Science Letters* **38**, 1–25.

Atherton MP and Petford N (1993) Generation of sodium-rich magmas from newly underplated basaltic crust. *Nature* **362**, 144–6.

Bao PS, Xiao XC, Su L and Wang J (2007) Geochemical characteristics and isotopic dating for the Dongcuo Ophiolite, Tibet Platea. *Science in China: Series D: Earth Sciences* **37**, 298–307 (in Chinese with English abstract).

Barry TL, Pearce JA, Leat PT, Millar IL and Le Roex AP (2006) Hf isotope evidence for selective mobility of high-field-strength elements in a subduction setting: South Sandwich Islands. *Earth and Planetary Science Letters* **252**, 223–44.

Baxter AT, Aitchison JC and Zyabrev SV (2009) Radiolarian age constraints on Mesotethyan ocean evolution, and their implications for development of the Bangong-Nujiang suture, Tibet. *Journal of the Geological Society* **166**, 689–94.

Ben Othman D, White WM and Patchett J (1989) The geochemistry of marine sediments, island arc magma genesis and crust-mantle recycling. *Earth and Planetary Science Letters* **94**, 1–21.

Bignold SM and Treloar PJ (2003) Northward subduction of the Indian Plate beneath the Kohistan island arc, Pakistan Himalaya: new evidence from isotopic data. *Journal of the Geological Society, London* **160**, 377–84.

Castillo PR (2012) Adakite petrogenesis. *Lithos* **134–135**, 304–16.

Castillo PR, Janney PE and Solidum RU (1999) Petrology and geochemistry of Camiguin Island, southern Philippines: insights to the source of adakites and other lavas in a complex arc setting. *Contributions to Mineralogy and Petrology* **134**, 33–51.

Chang QS, Zhu DC, Zhao ZD, Dong GC, Mo XX, Liu YS and Hu ZC (2011) Zircon U-Pb geochronology and Hf isotopes of the Early Cretaceous Rena-Co rhyolites from southern margin of Qiangtang, Tibet, and their implications. *Acta Petrologica Sinica* **27**, 2034–44 (in Chinese with English Abstract).

Chen HA, Zhu XP, Ma DF, Huang HX, Li GM, Li YB, Li YC, Wei LJ and Liu CQ (2013) Geochronology and geochemistry of the Bolong Porphyry Cu-Au Deposit, Tibet and its mineralizing significance. *Acta Geologica Sinica* **87**, 1593–611 (in Chinese with English abstract).

Chen WY, Hu XC, Zhong Y, Fu YB, Li F and Wang YG (2018) Comment on "Sedimentary and tectonic evolution of the Southern Qiangtang Basin: implications for the Lhasa-Qiangtang Collision Timing" by A. Ma et al. *Journal of Geophysical Research: Solid Earth* **123**, 7338–42.

Chiu HY, Chung SL, Wu FY, Liu DY, Liang YH, Lin IJ, Iizuka Y, Xie LW, Wang YB and Chu MF (2009) Zircon U-Pb and Hf isotopic constraints from eastern Transhimalayan batholiths on the precollisional magmatic and tectonic evolution in southern Tibet. *Tectonophysics* **477**, 3–19.

Chung SL, Chu MF, Zhang Y, Xie Y, Lo CH, Lee TY, Lan CY, Li X, Zhang Q and Wang Y (2005) Tibetan tectonic evolution inferred from spatial and temporal variations in post-collisional magmatism. *Earth Science Reviews* **68**, 173–96.

Chung SL, Liu DY, Ji JQ, Chu MF, Lee HY, Wen DJ, Lo CH, Lee TY, Qian Q, Zhang Q (2003) Adakites from continental collision zones: melting of thickened lower crust beneath southern Tibet. *Geology* **31**, 1021–4.

Collins WJ, Beams SD, White AJR and Chappell BW (1982) Nature and origin of A-type granites with particular reference to southeastern Australia. *Contributions to Mineralogy and Petrology* **80**, 189–200.

Condie KC (2001) *Mantle Plume and Their Record in Earth History*. London: Cambridge University Press.

Corfu F, Hanchar JM, Hoskin PWO and Kinny P (2003) Atlas of zircon textures. *Reviews in Mineralogy and Geochemistry* **53**, 469–500.

Defant MJ and Drummond MS (1990) Derivation of some modern arc magmas by melting of young subducted lithosphere. *Nature* **347**, 662–5.

Defant MJ and Kepezhinskas P (2001) Evidence suggests slab melting in arc magmas. *EOS Transactions American Geophysical Union* **82**, 65–9.

Defant MJ, Xu JF, Kepezhinskas P, Wang Q, Zhang Q and Xiao L (2002) Adakites: some variations on a theme. *Acta Petrologica Sinica* **18**, 129–42.

Dewey JF, Shackleton RM, Chang C and Sun Y (1988) The tectonic evolution of the Tibetan plateau. *Philosophical Transactions of the Royal Society B Biological Sciences* **327**, 379–413.

Dokuz A, Uysal İ, Meisel W, Turan M, Duncan R and Akçay M (2013) Post-collisional adakitic volcanism in the eastern part of the Sakarya Zone, Turkey: evidence for slab and crustal melting. *Contributions to Mineralogy and Petrology* **166**, 1443–68.

Elliott T, Plank T, Zindler A, White W and Bourdon B (1997) Element transport from slab to volcanic front at the Mariana arc. *Journal of Geophysical Research - Solid Earth* **102**, 14991–5019.

Fan JJ, Li C, Wang M and Xie CM (2018) Reconstructing in space and time the closure of the middle and western segments of the Bangong Tethyan Ocean in the Tibetan Plateau. *International Journal of Earth Sciences* **107**, 1–19.

Fan JJ, Li C, Xie CM and Wang M (2014) Petrology, geochemistry, and geochronology of the Zhonggang ocean island, northern Tibet: implications for the evolution of the Banggongco-Nujiang oceanic arm of the Neo-Tethys. *International Geology Review* **56**, 1504–20.

Feeley TC and Hacker MD (1995) Intracrustal derivation of Na-rich andesitic and dacitic magmas — an example from volcan Ollague, Andean central volcanic zone. *Journal of Geology* **103**, 213–25.

Gao S, Rudnick RL, Yuan HL, Liu XM, Liu YS, Xu WL, Lin WL, Ayers J, Wang XC and Wang QH (2004) Recycling lower continental crust in the North China craton. *Nature* **432**, 892–97.

Girardeau J, Marcoux J, Allegre CJ, Bassoullet JP, Tang Y, Xiao X, Zao Y and Wang X (1984) Tectonic environment and geodynamic significance of the Neo-Cimmerian Donqiao Ophiolite, Bangong-Nujiang suture zone, Tibet. *Nature* **307**, 27–31.

Griffin WL, Wang X, Jackson SE, Pearson NJ, O'Reilly SY, Xu XS and Zhou XM (2002) Zircon chemistry and magma mixing, SE China: in-situ analysis of Hf isotopes, Tonglu and Pingtan igneous complexes. *Lithos* **61**, 237–69.

Guo ZF, Wilson M and Liu JQ (2007) Post-collisional adakites in south Tibet: products of partial melting of subduction-modified lower crust. *Lithos* **96**, 205–24.

Guynn JH, Kapp P, Pellen A, Heizer M, Gehrels G and Ding L (2006) Tibetan basement rocks near Amdo reveal "missing" Mesozoic tectonism along the Bangong suture, central Tibet. *Geology* **34**, 505–8.

Hao LL, Wang Q, Wyman DA, Ou Q, Dan W, Jiang ZQ, Wu FY, Yang JH, Long XP and Li J (2016a) Underplating of basaltic magmas and crustal growth in a continental arc: evidence from Late Mesozoic intermediate-felsic intrusive rocks in southern Qiangtang, central Tibet. *Lithos* **245**, 223–42.

Hao LL, Wang Q, Wyman DA, Ou Q, Dan W, Jiang ZQ, Yang JH, Li J and Long XP (2016b) Andesitic crustal growth via m elange partial melting: evidence from Early Cretaceous arc dioritic/andesitic rocks in southern Qiangtang, central Tibet. *Geochemistry, Geophysics Geosystems* **17**, 1641–59.

Hart SR (1984) A large-scale isotope anomaly in the Southern Hemisphere mantle. *Nature* **309**, 753–7.

Hawkesworth CJ, Gallagher K, Hergt JM and Mcdermott F (1993) Mantle and slab contributions in arc magmas. *Annual Review of Earth and Planetary Sciences* **21**, 175–204.

Hofmann AW (1997) Mantle geochemistry: the message from oceanic volcanism. *Nature* **385**, 219–29.

Hofmann AW (2003) Sampling mantle heterogeneity through oceanic basalts: isotopes and trace elements. In *The Mantle and Core. Treatise on Geochemistry* (ed. RW Carlson), pp. 61–101. Oxford: Elservier-Pergamon.

Hoskin PWO and Schaltegger U (2003) The composition of zircon and igneous and metamorphic petrogenesis. *Reviews in Mineralogy and Geochemistry* **53**, 27–62.

Hou ZQ, Gao YF, Qu XM, Rui ZY and Mo XX (2004). Origin of adakitic intrusives generated during mid-Miocene east-west extension in southern Tibet. *Earth and Planetary Science Letters* **220**, 139–55.

Hsu KJ, Pan GT and Sengor AMC (1995) Tectonic evolution of the Tibetan plateau: a working hypothesis based on the archipelago model of orogensis. *International Geology Review* **37**, 473–508.

Hu XM, Ma AL, Xue WW, Garzanti E, Cao Y, Li SM, Sun GY and Lai W (2022) Exploring a lost ocean in the Tibetan Plateau: birth, growth, and demise of the Bangong-Nujiang Ocean. *Earth-Science Reviews* **229**, 104031.

Hugh RR (1993) *Using Geochemical Data: Evaluation, Presentation, Interpretation*. New York: Longman Group UK Ltd, 352 p.

Kapp P, DeCelles PG, Gehrels GE, Heizler M and Ding L (2007) Geological records of the Lhasa-Qiangtang and Indo-Asian collisions in the Nima area of central Tibet. *Geological Society of America Bulletin* **119**, 917–32.

Kapp P, Yin A, Harrison TM and Ding L (2005) Cretaceous-Tertiary shortening, basin development, and volcanism in central Tibet. *Geological Society of America Bulletin* **117**, 865–78.

Kapp P, Yin A, Manning CE, Harrison TM and Taylor MH (2003) Tectonic evolution of the early Mesozoic blueschist-bearing Qiangtang metamorphic belt, central Tibet. *Tectonics* **22**, 1043.

Karsli O, Dokuz A, Kandemir R, Aydin F, Schmitt AK, Ersoy EY and Alyıldız C (2019) Adakitic parental melt generation by partial fusion of the juvenile lower crust, Sakarya Zone, NE Turkey: a far-field response to break-off of the southern Neotethyan oceanic lithosphere. *Lithos* **338–339**, 58–72.

Karsli O, Dokuz A, Uysal I, Aydin F, Kandemir R, Wijbrans RJ (2010) Generation of the early Cenozoic adakitic volcanism by partial melting ofmafic lower crust, Eastern Turkey: implications for crustal thickening to delamination. *Lithos* **114**, 109–20.

Kay RW and Kay SM (1993) Delamination and delamination magmatism. *Tectonophysics* **219**, 177–89.

Kelemen PB, Hanghøj K and Greene AR. (2003) One view of the geochemistry of subduction-related magmatic arcs, with an emphasis on primitive andesite and lower crust. In *Treatise on Geochemistry* (ed. RL Rudnick), pp. 593–659. Amsterdam: Elsevier, 3.

Kemp AIS, Hawkesworth CJ, Foster GL, Paterson BA,Woodhead JD, Hergt JM, Gray CM and Whitehouse MJ (2007) Magmatic and crustal differentiation history of granitic rocks from Hf-O isotopes in zircon. *Science* **315**, 980–3.

Kimura JI, Gill JB, Kunikiyo T, Osaka I, Shimoshioiri Y, Katakuse M, Kakubuchi S, Nagao T, Furuyama K, Kamei A, Kawabata H, Nakajima J, van Keken PE and Stern RJ (2014) Diverse magmatic effects of subducting a hot slab in SW Japan: results from forward modeling. *Geochemistry, Geophysics, Geosystems* **15**, 691–739.

Lai SC and Qin JF (2008) Petrology and geochemistry of the granulite xenoliths from Cenozoic Qiangtang volcanic field: implication for the nature of the lower crust in the northern Tibetan plateau and the genesis of Cenozoic volcanic rocks. *Acta Petrologica Sinica* **24**, 325–36 (in Chinese with English abstract).

Lai SC, Qin JF and Li YF (2007) Partial melting of thickened Tibetean Crust: geochemical evidence from Cenozoic adakitic volcanic rocks. *International Geology Review* **49**, 357–73.

Li JX, Qin KZ, Li GM, Richards JP, Zhao JX and Cao MJ (2014a) Geochronology, geochemistry, and zircon Hf isotopic compositions of Mesozoic intermediate-felsic intrusions in central Tibet: petrogenetic and tectonic implications. *Lithos* **198–199**, 77–91.

Li JX, Qin KZ, Li GM, Xiao B, Zhao JX, Cao MJ and Chen L (2013a) Petrogenesis of ore-bearing porphyries from the Duolong porphyry Cu-Au deposit, central Tibet: evidence from U-Pb geochronology, petrochemistry and Sr-Nd-Hf-O isotope characteristics. *Lithos* **160**, 216–27.

Li JX, Qin KZ, Li GM, Xiao B, Zhao JX, Chen L (2016) Petrogenesis of Cretaceous igneous rocks from the Duolong porphyry Cu-Au deposit, central Tibet: evidence from zircon U-Pb geochronology, petrochemistry and Sr-Nd-Pb-Hf isotope characteristics. *Geological Journal* **51**, 216–27.

Li SM, Zhu DC, Wang Q, Zhao ZD, Sui QL, Liu SA, Liu D, Mo XX (2014b) Northward subduction of Bangong-Nujiang Tethys: insight from Late Jurassic intrusive rocks from Bangong Tso in western Tibet. *Lithos* **205**, 284–97.

Li YL, He J, Wang CS, Han ZP, Ma PF, Xu M and Du KY (2015) Cretaceous volcanic rocks in south qiangtang terrane: products of northward subduction of the bangong-nujiang ocean? *Journal of Asian Earth Sciences* **104**, 69–83.

Li YL, He J, Wang CS, Santosh M, Dai JG, Zhang YX, Wei YS and Wang JG (2013b) Late Cretaceous k-rich magmatism in central Tibet: evidence for early elevation of the Tibetan plateau? *Lithos* **160–161**, 1–13.

Liu S, Hu R Z, Gao S, Feng CX, Coulson IM, Feng GY, Qi YQ, Yang YH, Yang CG and Tang L (2012) U-Pb zircon age, geochemical and Sr-Nd isotopic data as constraints on the petrogenesis and emplacement time of andesites from Gerze, southern Qiangtang Block, northern Tibet. *Journal of Asian Earth Sciences* **45**, 150–61.

Liu S, Hu RZ, Feng CX, Zhou HB, Li C, Chi XG, Peng JT, Zhong H, Qi L, Qi YQ and Wang T (2008) Cenozoic high Sr/Y volcanic rocks in the Qiangtang terrane, northern Tibet: geochemical and isotopic evidence for the origin of delaminated lower continental melts. *Geological Magazine* **145**, 463–74.

Liu WL, Xia B, Zhong Y, Cai JX, Li JF, Liu HF, Cai ZR and Sun ZL (2014) Age and composition of the Rebang Co and Julu ophiolites, central Tibet: implications for the evolution of the Bangong Meso-Tethys. *International Geology Review* **56**, 430–47.

Luo AB, Fan JJ, Hao YJ, Li H and Zhang BC (2020) Aptian flysch in Central Tibet: constraints on the timing of closure of the Bangong-Nujiang Tethyan Ocean. *Tectonics* **39**, e2020TC006198.

Macpherson CG, Dreher ST and Thirlwall MF (2006) Adakites without slab melting: high pressure differentiation of island arc magma, Mindanao, the Philippines. *Earth and Planetary Science Letters* **243**, 581–93.

Mahoney JJ, Frei R, Tejada MLG, Mo XX, Leat PT and Nägler TF (1998) Tracing the Indian Ocean mantle domain through time: isotope results from old West Indian, East Tethyan, and South Pacific seafloor. *Journal of Petrology* **39**, 1285–306.

Maniar PD and Piccoli PM (1989) Tectonic discrimination of granitoids. *Geological Society of America Bulletin* **101**, 635–43.

Martin H, Smithies RH, Rapp R, Moyen JF, Champion D (2005) An overview of adakite, tonalite-trondhjemite-granodiorite (TTG), and sanukitoid: relationships and some implications for crustal evolution. *Lithos* **79**, 1–24.

Middlemost EAK (1994) Naming materials in the magma/igneous rock system. *Earth-Science Reviews* **37**, 215–24.

Miller C, Schuster R, Klotzli U, Frank W and Purtscheller F (1999) Post-collisional potassic and ultra-potassic magmatism in SW Tibet, geochemical, Sr-Nd-Pb-O isotopic constraints for mantle source characteristics and petrogenesis. *Journal of Petrology* **66**, 699–715.

Mo X, Zhao Z, Deng J, Flower M, Yu X, Luo Z, Li Y, Zhou S, Dong S, Zhu D and Wang L (2006) Petrology and geochemistry of postcollisional volcanic rocks from the Tibetan plateau: implications for lithosphere heterogeneity and collision-induced asthenospheric mantle flow. In: Dilek, Y., Pavlides, S. (Eds.), Postcollisional Tectonics and Magmatism in the Mediterranean Region and Asia. *Geological Society of America Special Paper* 409, 507–530.

Mo XX, Hou ZQ, Niu YL, Dong GC, Qu XM, Zhao ZD and Yang ZM (2007) Mantle contributions to crustal thickening during continental collision: evidence from Cenozoic igneous rocks in southern Tibet. *Lithos* **96**, 225–42.

Murphy MA, Yin A, Harrison TM, Dürr SB, Chen Z, Ryerson FJ, Kidd WSF, Wang X and Zhou X (1997) Did the Indo-Asian collision alone create the Tibetan plateau? *Geology* **25**, 719–22.

Nakakuki T and Mura E (2013) Dynamics of slab rollback and induced back-arc basin formation. *Earth and Planetary Science Letters* **361**, 287–97.

Niu YL and Batiza R (1997) Trace element evidence from seamounts for recycled oceanic crust in the Eastern Pacific mantle. *Earth and Planetary Science Letters* **148**, 471–83.

Pan GT, Ding J, Yao DS and Wang LQ (2004) The geological map of the Qinghai-Xizang (Tibet) and adjacent areas, Chengdu Institute of Geology and Mineral Resource and China Geological Survey. Chengdu Map Press, Chengdu, scale 1:1,500,000 (in Chinese).

Pearce JA (1982) *Trace element characteristics of lavas from destructive plate boundaries.// Andesites: orogenic andesites and related rocks*. New York: John Wiley and Sons, 525–548 pp.

Pearce JA and Deng W (1988) The ophiolites of the Tibet geotraverse, Lhasa to Golmud (1985) and Lhasa to Kathmandu (1986). *Philosophical Transactions of the Royal Society A Mathematical Physical and Engineering Sciences* **327**, 215–38.

Pearce JA, Harris NBW and Tindle AG (1984) Trace element discrimination diagrams for the tectonic interpretation of granitic rocks. *Journal of Petrology* **25**, 956–83.

Pearce JA and Peate DW (1995) Tectonic implications of the composition of volcanic arc magmas. *Annual Review of Earth and Planetary Sciences* **23**, 251–85.

Peccerillo A and Taylor SR (1976) Geochemistry of Eocene calc-alkaline volcanic-rocks from Kastamonu district, northern Turkey. *Contributions to Mineralogy and Petrology* **58**, 63–81.

https://doi.org/10.1017/S0016756823000274 Published online by Cambridge University Press

Plank T (2005) Constraints from thorium/Lanthanum on Sediment Recycling at Subduction Zones and the Evolution of the Continents. *Journal of Petrology* **16**, 921–44.

Plank T and Langmuir CH (1998) The chemical composition of subducting sediment and its consequences for the crust and mantle. *Chemical Geology* **145**, 325–94.

Rapp RP, Shimizu N and Norman MD (2003) Growth of early continental crust by partial melting of eclogite. *Nature* **425**, 605–9.

Rapp RP, Shimizu N, Norman MD and Applegate GS (1999) Reaction between slab derived melts and peridotite in the mantle wedge: experimental constraints at 3.8 GPa. *Chemical Geology* **160**, 335–56.

Rapp RP and Watson EB (1995) Dehydration melting of metabasalt at 8-32 kbar: implica-tions for continental growth and crust-mantle recycling. *Journal of Petrology* **36**, 891–931.

Raterman NS, Robinson AC and Cowgill ES (2014) Structure and detrital zircon geochronology of the Domar fold-thrust belt: evidence of pre-Cenozoic crustal thickening of the western Tibetan Plateau. *Geological Society of America, Special Paper* **507**, 89–114.

Richards JP (2003) Tectono-magmatic precursors for porphyry Cu-(Mo-Au) deposit formation. *Ecomomic Geology* **98**, 1515–33.

Richards JP and Kerrich R (2007) Special Paper: adakite-like rocks; Their diverse origins and questionable role in metallogenesis. *Economic Geology* **102**, 537–76.

Rolland Y, Picard C, Pecher A, Lapierre H, Bosch D and Keller F (2002) The Cretaceous Ladakh arc of NW Himalaya: slab melting and mantle interaction during fast northward drift of Indian Plate. *Chemical Geology* **182**, 139–78.

Sengör AMC (1979) Mid-Mesozoic closure of Permo-Triassic Tethys and its implications. *Nature* **279**, 590–3.

She HQ, Li JW, Ma DF, Li GM, Zhang DQ, Feng CY, Qu WJ and Pan GT (2009) Molybdenite Re-Os and SHRIMP zircon U-Pb dating of Duobuza porphyry copper deposit in Tibet and its geological implications. *Mineral Deposits* **28**, 737–46 (in Chinese with English abstract).

Shi HZ, Li YC, Huang HX, Liu H, Huang Y, Li GM, Zhang LK, Ma DF and Li YB (2019) Genesis of early cretaceous Meiriqiecuo formation volcanic rocks in the Duolong ore concentration area, southern margin of Qiangtang, Tibet, China. *Journal of Chengdu University of Technology (Science & Technology Edition)* **46**, 421–34 (in Chinese with English abstract).

Shi LZ, Huang JY and Chen W (2020) Birth and demise of the Bangong–Nujiang Tethyan Ocean: a review from the Gerze area of Central Tibet: Comment. *Earth-Science Reviews* **208**, 103209.

Shi RD, Yang JS, Xu ZQ and Qi XX (2008) The Bangong Lake ophiolite (NW Tibet) and its bearing on the tectonic evolution of the Bangong-Nujiang suture zone. *Journal of Asian Earth Sciences* **32**, 438–57.

Song Y, Chen W, Wei SG, Ma XD, Sun M and Liu QP (2021) Evolution of continental arc at root caused by igneous garnet and amphibole fractionation: evidence from Jurassic intermediate-felsic intrusive rocks in southern Qiangtang, Tibet. *Lithos* **382–383**, 105935.

Stern CR and Kilian R (1996) Role of the subducted slab, mantle wedge and continental crust in the generation of adakites from the Andean austral volcanic zone. *Contributions to Mineralogy and Petrology* **123**, 263–81.

Streck MJ, Leeman WP and Chesley J (2007) High-magnesian andesite from Mount Shasta: a product of magma mixing and contamination, not a primitive mantle melt. *Geology* **35**, 351–4.

Sui QL, Wang Q, Zhu DC, Zhao ZD, Chen Y, Santosh M, Hu ZC, Yuan HL and Mo XX (2013) Compositional diversity of ca. 110 Ma magmatism in the northern Lhasa Terrane, Tibet: implications for the magmatic origin and crustal growth in a continent-continent collision zone. *Lithos* **168–169**, 144–59.

Sun J (2015) Magmatism and Metallogenesis at Duolong Ore District, Tibet. A Dissertation Submitted to China University of Geosciences for Doctoral Degree, Beijing. 1–199 (in Chinese with English abstract)

Sun SS and McDonough WF (1989) Chemical and isotopic systematics of oceanic basalts: implications for mantle composition and processes. *Geological Society of London Special Publications* **42**, 313–45.

Tang GJ, Wang Q, Wyman DA, Li ZX, Zhao ZH, Jia XH and Jiang ZQ (2010) Ridge subduction and crustal growth in the central Asian Orogenic Belt: evidence from Late Carboniferous adakites and high-Mg diorites in the western Junggar region, northern Xinjiang (West China). *Chemical Geology* **277**, 281–300.

Tsuchiya N, Suzuki S, Kimura JI and Kagami H (2005) Evidence for slab melt/mantle reaction: petrogenesis of Early Cretaceous and Eocene high-Mg andesites from the Kitakami Mountains, Japan. *Lithos* **79**, 179–206.

van de Zedde DMA and Wortel MJR (2001) Shallow slab detachment as a transient source of heat at midlithospheric depth. *Tectonics* **20**, 868–82.

Vroon PZ, van Bergen MJ, Klaver GJ and White WM (1995) Strontium, neodymium, and lead isotopic and trace-element signatures of the East Indonesian sediments: provenance and implications for Banda Arc magma genesis. *Geochimica et Cosmochimica Acta* **59**, 2573–98.

Wang BD, Wang LQ, Chung SL, Chen JL, Yin FG, Liu H, Li XB and Chen LK (2016) Evolution of the Bangong-Nujiang Tethyan ocean: insights from the geochronology and geochemistry of mafic rocks within ophiolites. *Lithos* **245**, 18–33.

Wang Q, McDermott F, Xu JF, Bellon H and Zhu YT (2005) Cenozoic K-rich adakitic volcanic rocks in the Hohxil area, northern Tibet: lower-crustal melting in an intracontinental setting. *Geology* **33**, 465–8.

Wang Q, Tang JX, Fang X, Lin B, Song Y, Wang YY, Yang HH, Yang C, Li YH, Wei LJ, Feng J and Li L (2015) Petrogenetic setting of andsites in Rongna ore block, Tiegelong Cu (Au-Ag) deposit, Duolong ore concentration area, Tibet: evidence from zircon U-Pb LA-ICP-MS dating and petrogeochemistry of andsites. *Geology in China* **42**, 1324–36 (in Chinese with English abstract).

Wang Q, Wyman DA, Xu JF, Dong YH, Vasconcelos PM, Pearson N, Wan Y, Dong H, Li CF, Yu YS, Zhu TX, Feng XT, Zhang QY, Zi F and Chu ZY (2008a) Eocene melting of subducting continental crust and early uplifting of central Tibet: evidence from central-western Qiangtang high-K calc-alkaline andesites, dacites and rhyolites. *Earth and Planetary Science Letters* **272**, 158–71.

Wang Q, Wyman DA, Xu JF, Wan YS, Li CF, Zi F, Jiang ZQ, Qiu HN, Chu ZY, Zhao ZH and Dong YH (2008b) Triassic Nb-enriched basalts, magnesian andesites, and adakites of the Qiangtang terrane (Central Tibet): evidence for metasomatism by slab-derived melts in the mantle wedge. *Contributions to Mineralogy and Petrology* **155**, 473–90.

Wang Q, Wyman DA, Xu JF, Zhao ZH, Jian P, Xiong XL, Bao ZW, Li CF and Bai ZH (2006a) Petrogenesis of Cretaceous adakitic and shoshonitic igneous rocks in the Luzong area, Anhui Province (eastern China): implications for geodynamics and Cu-Au mineralization. *Lithos* **89**, 424–46.

Wang Q, Xu JF, Jian P, Bao ZW, Zhao ZH, Li CF, Xiong XL and Ma JL (2006b) Petrogenesis of adakitic porphyries in an extensional tectonic setting, Dexing, South China: implications for the genesis of porphyry copper mineralization. *Journal of Petrology* **47**, 119–44.

Wei SG, Song Y, Tang JX, Liu ZB, Wang Q, Lin B, Feng J, Hou L, Danzhen WX (2018) Geochronology, geochemistry, Sr-Nd-Hf isotopic compositions, and petrogenetic and tectonic implications of Early Cretaceous intrusions associated with the Duolong porphyry-epithermal Cu-Au deposit, central Tibet. *International Geology Review* **60**, 1116–39.

Wei SG, Tang JX, Song Y, Liu ZB, Feng J and Li YB (2017) Early cretaceous bimodal volcanism in the duolong Cu mining district, western Tibet: record of slab breakoff that triggered Ca. 108–113 Ma magmatism in the western Qiangtang terrane. *Journal of Asian Earth Sciences* **138**, 588–607.

Wilson M (1989) *Igneous Petrogenesis*. London: Unwin Hyman.

Wood DA (1980) The application of a Th-Hf-Ta diagram to problems of tectonic magmatic classification on and to establishing the nature of crustal contamination of the British Tertiary volcanic province. *Earth and Planetary Science Letters* **50**, 11–30.

Woodhead JD, Hergt JM, Davidson JP and Eggins SM (2001) Hafnium isotope evidence for 'conservative' element mobility during subduction zone processes. *Earth and Planetary Science Letters* **192**, 331–46.

Xin HB, Qu XM, Wang RJ, Liu HF, Zhao YY and Huang W (2009) Geochemistry and Pb, Sr, Nd isotopic features of ore-bearing porphyries in Bangong Lake porphyry copper belt, Western Tibet. *Mineralium Deposita* **28**, 785–92 (in Chinese with English abstract).

https://doi.org/10.1017/S0016756823000274 Published online by Cambridge University Press

Xu JF, Shinjo R, Defant MJ, Wang Q and Rapp RP (2002) Origin of Mesozoic adakitic intrusive rocks in the Ningzhen area of east China: partial melting of delaminated lower continental crust? *Geology* **30**, 1111–4.

Xu RH, Schärer U and Allègre CJ (1985) Magmatism and metamorphism in the Lhasa Block (Tibet): a geochronological study. *Journal of Geology* **93**, 41–57.

Xu W, Li C, Xu MJ, Wu YW, Fan JJ and Wu H (2015) Petrology, geochemistry, and geochronology of boninitic dikes from the Kangqiong ophiolite: implications for the early cretaceous evolution of Bangong–Nujiang Neo-Tethys Ocean in Tibet. *International Geology Review* **57**, 2028–43.

Yin A and Harrison TM (2000) Geological evolution of the Himalayan-Tibetan orogen. *Annual Review of Earth and Planetary Sciences* **28**, 211–80.

Yin JX, Xu JT, Liu CJ and Li H (1988) The Tibetan Plateau: regional stratigraphic context and previous work. *Philosophical Transactions of the Royal Society of London. Series A Mathematical and Physical Sciences* **327**, 5–52.

Zeng YC, Xu JF, Chen JL, Wang BD, Huang F, Xia XP and Li MJ (2021) Early Cretaceous (~138–134 Ma) forearc ophiolite and tectonomagmatic patterns in central Tibet: subduction termination and re-initiation of Meso-Tethys Ocean caused by collision of an oceanic plateau at the continental margin? *Tectonics* **40**, e2020TC006423.

Zhang KJ, Xia B, Zhang YX, Liu WL, Zeng L, Li JF and Xu LF (2014) Central Tibetan Meso-Tethyan oceanic plateau. *Lithos* **210**, 278–88.

Zhang KJ, Zhang YX, Tang XC and Xia B (2012) Late Mesozoic tectonic evolution and growth of the Tibetan plateau prior to the Indo-Asian collision. *Earth-Science Reviews* **114**, 236–49.

Zhang SQ, Mahoney JJ, Mo XX, Ghazi AM, Milani L, Crawford AJ, Guo TY and Zhao ZD (2005) Evidence for a widespread Tethyan upper mantle with Indian-Ocean-type isotopic characteristics. *Journal of Petrology* **46**, 829–58.

Zhu DC, Li SM, Cawood PA, Wang Q, Zhao ZD, Liu SA, and Wang LQ (2016) Assembly of the Lhasa and Qiangtang terranes in central Tibet by divergent double subduction. *Lithos*, **245**, 7–17.

Zhu DC, Pan GT, Chung SL, Liao ZL, Wang LQ and Li GM (2008) Shrimp zircon age and geochemical constraints on the origin of lower Jurassic volcanic rocks from the yeba formation, southern Gangdese, south Tibet. *International Geology Review* **50**, 442–71.

Zhu DC, Pan GT, Mo XX, Wang LQ, Zhao ZD and Liao ZL (2006) Identification of the Mesozoic OIB-type basalts in central Qinghai-Tibetan Plateau: geochronology, geochemistry and their tectonic setting. *Acta Geological Sinica* **80**, 1312–28 (in Chinese with English abstract).

Zhu DC, Zhao ZD, Pan GT, Lee HY, Kang ZQ, Liao ZL, Wang LQ, Li GM, Dong GC and Liu B (2009) Early cretaceous subduction-related adakite-like rocks of the Gangdese Belt, southern Tibet: products of slab melting and subsequent melt- peridotite interaction? *Journal of Asian Earth Sciences* **34**, 298–309.

Zhu XP, Chen HA, Liu HF, Ma DF, Li GM, Zhang H, Liu CQ and Wei LJ (2015) Geochronology and geochemistry of porphyries from the Naruo porphyry copper deposit, Tibet and their metallogenic signifificance. *Acta Petrologica Sinica* **89**, 109–28 (in Chinese with English abstract).

Zindler A and Hart SR (1986) Chemical geodynamics. *Annual Review of Earth and Planetary Sciences* **14**, 493–571.